Article

Unraveling the Origin of the Peculiar Reaction Field of Triruthenium Ring Core Structures

Athanassios C. Tsipis, Christos E. Kefalidis, and Constantinos A. Tsipis

J. Am. Chem. Soc., **2007**, 129 (45), 13905-13922• DOI: 10.1021/ja074094p • Publication Date (Web): 23 October 2007

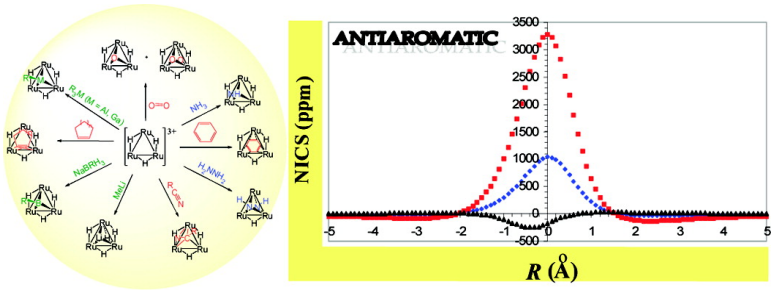

More About This Article

Additional resources and features associated with this article are available within the HTML version:

- Supporting Information
- Links to the 2 articles that cite this article, as of the time of this article download
- Access to high resolution figures
- Links to articles and content related to this article
- Copyright permission to reproduce figures and/or text from this article

View the Full Text HTML

J|A|C|S
ARTICLES
Published on Web 10/23/2007

Unraveling the Origin of the Peculiar Reaction Field of Triruthenium Ring Core Structures

Athanassios C. Tsipis,*,† Christos E. Kefalidis,‡ and Constantinos A. Tsipis*,‡

Contribution from the Laboratory of Inorganic and General Chemistry, Department of Chemistry, University of Ioannina, 451 10 Ioannina, Greece, and Laboratory of Applied Quantum Chemistry, Faculty of Chemistry, Aristotle University of Thessaloniki, 541 24 Thessaloniki, Greece

Received June 6, 2007; E-mail: tsipis@chem.auth.gr; attsipis@cc.uoi.gr

Abstract: The molecular and electronic structures, stabilities, bonding features, and spectroscopic properties of prototypical ligand stabilized [*cyclo*-$Ru_3(\mu_2\text{-}X)_3]^{0,3+}$ (X = H, BH, CH_2, NH_2, OH, Cl, NH, CO, O, PH_2, CF_2, CCl_2, CNH, N_3) isocycles have been thoroughly investigated by means of electronic structure calculation methods at the DFT level of theory. All [*cyclo*-$Ru_3(\mu_2\text{-}X)_3]^{0,3+}$ species, except [*cyclo*-$Ru_3(\mu_2\text{-}H)_3]^{3+}$, are predicted to be aromatic molecules. In contrast, the [*cyclo*-$Ru_3(\mu_2\text{-}H)_3]^{3+}$ species exhibits a high antiaromatic character, which would be responsible for the well-established peculiar reaction field of hydrido-bridged triruthenium core structures. The aromaticity/antiaromaticity of the model [*cyclo*-$Ru_3(\mu_2\text{-}X)_3]^{0,3+}$ isocycles was verified by an efficient and simple criterion in probing the aromaticity/antiaromaticity of a molecule, that of the nucleus-independent chemical shift, NICS(0), NICS(1), NICS(−1), $NICS_{zz}(1)$, and $NICS_{zz}(-1)$, along with the NICS scan profiles. The versatile chemical reactivity of the antiaromatic [*cyclo*-$Ru_3(\mu_2\text{-}H)_3]^{3+}$ molecule related to the activation of small molecules that leads to the breaking of various strong single and double bonds is thoroughly investigated by means of electronic structure computational techniques, and the mechanistic details for a representative activation process, that of the dehydrogenation of NH_3, to form a triply bridging imido-group (μ_3-NH) face-capping the Ru_3 ring are presented. Finally, the molecular and electronic structures, stabilities, and bonding features of a series of [*cyclo*-$Ru_3(\mu_2\text{-}H)_3(\mu_3\text{-}Nuc)]^{0,1,2+}$ (Nuc = BH, BCN, BOMe, C^{4-}, CH^{3-}, CMe^{3-}, N^{3-}, NH, N_3^-, NCO^-, OCN^-, NCS^-, O^{2-}, S^{2-}, OH^-, P^{3-}, POH^{2-}, Cl^-, O_2^{2-}, NCH, AlMe, GaMe, C_6H_6, and *cyclo*-C_3H_2Me) products formed upon reacting the archetype [*cyclo*-$Ru_3(\mu_2\text{-}H)_3]^{3+}$ molecule with the appropriate substrates are also comprehensibly analyzed.

Introduction

Metal−polyhydride cluster complexes effectively activate organic substrates in a unique manner, probably as a result of the cooperative action of the metal centers.[1,2] In particular, the interesting traits that are inherent to cyclopentadiene- or arene-stabilized trinuclear ruthenium polyhydride complexes involving a triangular trihydrido-bridged core structure have been extensively studied.[1,2] Their precursors formulated as [$(\eta^5\text{-}C_5Me_5)_3Ru_3(\mu\text{-}H)_3(\mu_3\text{-}H)_2$] and [$(\eta^6\text{-}C_6Me_6)_2(\eta^6\text{-}C_6H_6)Ru_3(\mu\text{-}H)_3]^+$ are electron-deficient species represented either by 2e-3c Ru−H−Ru bonds or by a Ru≡Ru triple bond with three hydrido bridges. Both electrophiles and nucleophiles were found to multiply coordinate to the 3-membered ruthenium ring, affording novel complexes exhibiting unprecedented catalytic activity toward selective activation of C−H, N−H, O−H, H−H, C−C, and C═C bonds and the hydrogenation of aromatics. Representative examples[1,2] of the reactivity of the [$(\eta^5\text{-}C_5Me_5)_3Ru_3(\mu\text{-}H)_3(\mu_3\text{-}H)_2$] cluster are shown in Scheme 1. Analogous reactivity exhibits the [$(\eta^6\text{-}C_6Me_6)_2(\eta^6\text{-}C_6H_6)Ru_3(\mu\text{-}H)_3]^+$ cluster as well. Very recently, density functional theory (DFT) study of hydride exchange in a binuclear polyhydride CpRu-(μ-H)$_4$RuCp complex

† University of Ioannina.
‡ Aristotle University of Thessaloniki.

(1) (a) Suzuki, H.; Tanaka, Y.; Takemori, T.; Tanaka, M. *J. Am. Chem. Soc.* **1994**, *116*, 10779. (b) Matsubara, K.; Okamura, R.; Tanaka, M.; Suzuki, H. *J. Am. Chem. Soc.* **1998**, *120*, 1108. (c) Inagaki, A.; Takemori, T.; Tanaka, M.; Suzuki, H. *Angew. Chem., Int. Ed.* **2000**, *39*, 404. (d) Ohki, Y.; Suzuki, H. *Angew. Chem., Int. Ed.* **2000**, *39*, 3463. (e) Takemori, T.; Inagaki, A.; Suzuki, H. *J. Am. Chem. Soc.* **2001**, *123*, 1762. (f) Suzuki, H.; Inagaki, A.; Matsubara, K.; Takemori, T. *Pure Appl. Chem.* **2001**, *73*, 315. (g) Okamura, R.; Tada, K.; Matsubara, K.; Oshima, M.; Suzuki, H. *Organometallics* **2001**, *20*, 4772. (h) Ohashi, M.; Matsubara, K.; Iizuka, T.; Suzuki, H. *Angew. Chem., Int. Ed.* **2003**, *42*, 937. (i) Nakajima, Y.; Inagaki, A.; Suzuki, H. *Organometallics* **2004**, *23*, 4040. (j) Takao, T.; Kakuta, S.; Tenjimbayashi, R.; Takemori, T.; Murotani, E.; Suzuki, H. *Organometallics* **2004**, *23*, 6090. (k) Takao, T.; Takaya, Y.; Murotani, E.; Tenjimbayashi, R.; Suzuki, H. *Organometallics* **2004**, *23*, 6094. (l) Nakajima, Y.; Suzuki, H. *Organometallics* **2005**, *24*, 1860. (m) Takao, T.; Kawashima, T.; Matsubara, K.; Suzuki, H. *Organometallics* **2005**, *24*, 3371. (n) Suzuki, H.; Kakigano, T.; Tada, K.; Igarashi, M.; Matsubara, K.; Inagaki, A.; Oshima, M.; Takao, T. *Bull. Chem. Soc. Jpn.* **2005**, *78*, 67. (o) Nakajima, Y.; Hajime, H.; Suzuki, H. *Angew. Chem., Int. Ed.* **2006**, *45*, 950.

(2) (a) Meister, G.; Rheinwald, G.; Stoekli-Evans, H.; Süss-Fink, G. *J. Chem. Soc., Dalton Trans.* **1994**, 3215. (b) Faure, M.; Jahncke, M.; Neels, A.; Stoekli-Evans, H.; Süss-Fink, G. *Polyhedron* **1999**, *18*, 2679. (c) Faure, M.; Vallins, A. T.; Stoekli-Evans, H.; Süss-Fink, G. *J. Organomet. Chem.* **2001**, *621*, 103. (d) Süss-Fink, G.; Faure, M.; Ward, T. R. *Angew. Chem., Int. Ed.* **2002**, *41*, 99. (e) Vieille-Petit, L.; Vallins, A. T.; Therrien, B.; Süss-Fink, G.; Ward, T. R. *J. Organomet. Chem.* **2003**, *684*, 117. (f) Süss-Fink, G.; Therrien, B.; Vieille-Petit, L.; Tschan, M.; Romakh, V. B;. Ward, T. R.; Dadras, M.; Laurenczy, G. *J. Organomet. Chem.* **2004**, *689*, 1362. (g) Vieille-Petit, L.; Karmazin-Brelot, L.; Labat, G.; Süss-Fink, G. *Eur. J. Inorg. Chem.* **2004**, 3907. (h) Hagen, C. M.; Vieille-Petit, L.; Laurenczy, G.; Süss-Fink, G.; Finke, R. G. *Organometallics* **2005**, *24*, 1819 and references therein. (i) Vieille-Petit, L.; Süss-Fink, G.; Therrien, B.; Ward, T. R.; Stoekli-Evans, H.; Labat, G.; Karmazin-Brelot, L.; Neels, A.; Bürgi, T.; Finke, R. G.; Hagen, C. M. *Organometallics* **2005**, *24*, 6104.

Scheme 1. Representative Examples of the Versatile Reactivity of the $[(\eta^5\text{-}C_5Me_5)_3Ru_3(\mu\text{-}H)_3(\mu_3\text{-}H)_2]$ Cluster

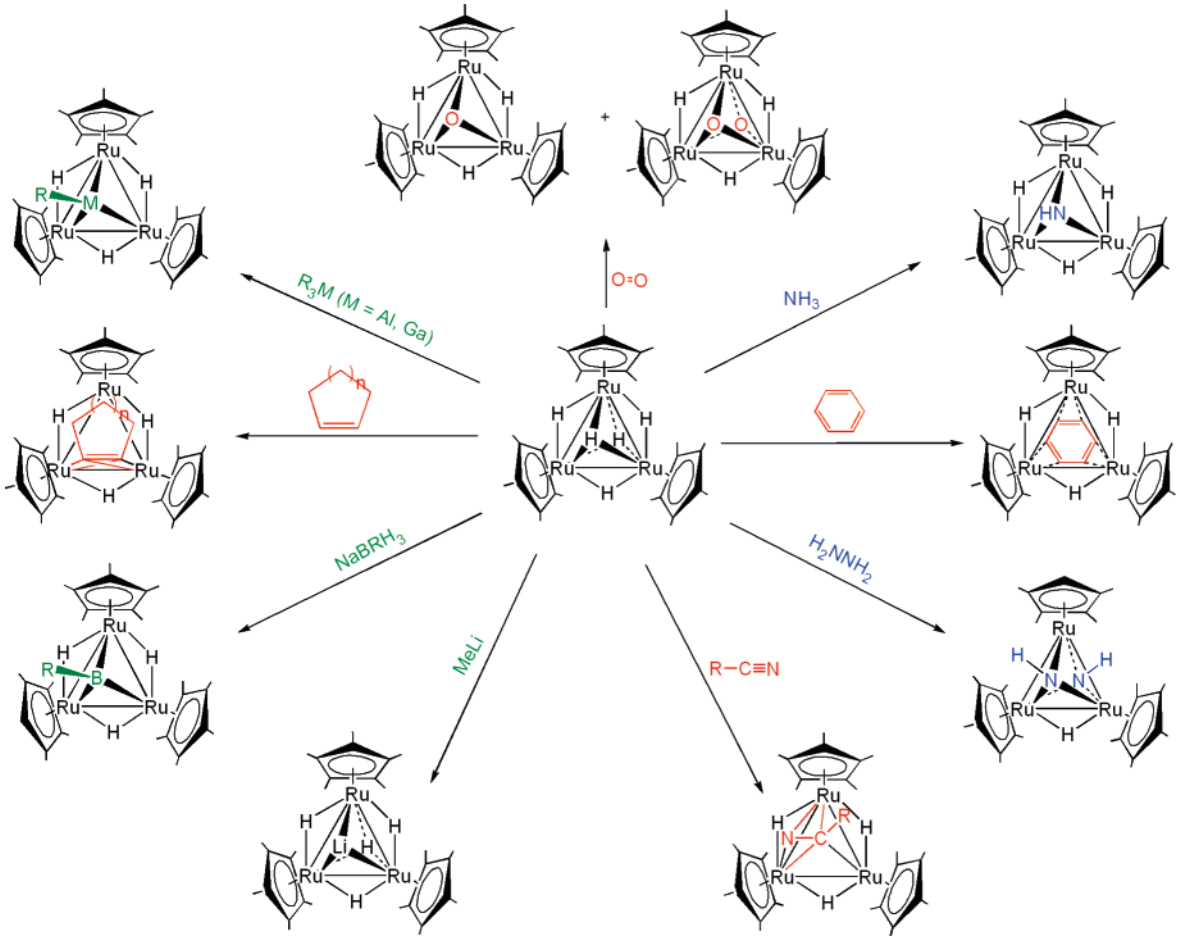

showed that the associative pathway is favored, but the details of the mechanism are rather complicated.[3]

Experimental and molecular modeling studies indicated that substrates are incorporated into the hydrophobic pocket spanned by the three cyclopentadiene or arene ligands in the triangular Ru_3 clusters. Therefore, the catalytic reactions occur within the host−guest complexes without prior coordination of the substrates ("supramolecular cluster catalysis").[2d,h] However, a number of catalyst−substrate host−guest complexes have been isolated and structurally well characterized.

A leading attribute of ruthenium and all of the transition elements is their penchant to aggregate in rings, cages, and clusters. An amazing common property of both the bare and ligand-stabilized ruthenium clusters is the unusual abundance of the triangular *cyclo*-Ru_3 and the square planar *cyclo*-Ru_4 rings.[1,2,4] Furthermore, despite the triangular ruthenium−polyhydride clusters, the fundamental triangular binary $Ru_3(CO)_{12}$ cluster is the parent compound of innumerable products.[5]

Catalyzed by the versatile reactivity and catalytic activity of the ruthenium−polyhydride clusters and the stunning growth of the aromaticity concept in "all-metal" aromatic rings,[6] we challenged to think about aromaticity/antiaromaticity in the triangular ligand-stabilized ruthenium(II) isocycles. In effect, we found that the 3-membered *cyclo*-ruthenium rings in a series of ligand stabilized $[cyclo\text{-}Ru_3(\mu_2\text{-}X)_3]^{0,3+}$ (X = BH, CH_2, NH_2, OH, Cl, NH, CO, O, PH_2, CF_2, CCl_2, CNH, N_3) clusters exhibited an unprecedented high diatropic response, thus being highly aromatic molecules. In contrast, the parent $[cyclo\text{-}Ru_3(\mu_2\text{-}H)_3]^{3+}$ species exhibits a high antiaromatic character, which would be responsible for the well-established peculiar reaction field of hydrido-bridged triruthenium core structures. Along this line, we predicted that nucleophilic substrates easily interact with the strongly antiaromatic electron deficient Ru_3 ring of the $[cyclo\text{-}Ru_3(\mu_2\text{-}H)_3]^{3+}$ species, forming stable adducts even in the absence of the hydrophobic pocket spanned by the stabilizing cyclopentadiene or arene ligands. We believe that the antiaromaticity of the Ru_3 rings might probably be the drive to account for their peculiar reaction field. Our own efforts have focused on demonstrating the Ru_3 cluster core's utility as a highly generalized synthon for use in a variety of applications and a standard bearer for the cluster revolution. In this context, we address a number of important issues related to the molecular and electronic structures, stabilities, bonding features, and

(3) Tussupbayev, S.; Vyboishchikov, S. F. *Organometallics* **2007**, *26*, 56.
(4) (a) Guo, R;. Balasubramanian, K. *J. Chem. Phys.* **2003**, *118*, 142. (b) Zhang, W.; Zhao, H.; Wang, L. *J. Phys. Chem. B* **2004**, *108*, 2140. (c) Scopelliti, S. G. R.; Severin, K. *Organometallics* **2005**, *24*, 5792. (d) Deeming, A. J.; Forth, C. S.; Hyder, Md. I.; Kabir, S. F.; Nordlander, E.; Rodgers, F.; Ullmann, B. *Eur. J. Inorg. Chem.* **2005**, 4352.
(5) (a) Delgado, E.; Donnadieu, B.; Hernandez, E.; Martin, M. P.; Zamora, F. *Acta Cryst.* **2002**, *E8*, m571. (b) Slebodnick, C.; Zhao, J.; Angel, R.; Hanson, B. E.; Song, Y.; Liu, Z.; Hemley, R. J. *Inorg. Chem.* **2004**, *43*, 5245. (c) Gervasio, G.; Bianchi, R.; Marabello, D. *Chem. Phys. Lett.* **2005**, *407*, 18. (d) Griffith, C. S.; Koutsantonis, G. A.; Skelton, B. W.; White, A. H. *J. Organomet. Chem.* **2005**, *690*, 3410. (e) Raithby, P. R.; Lewis, J.; Morewood, C. A.; Ramirez de Arellano M. C.; Shields, G. P. *J. Cluster Sci.* **2006**, *17*, 13.
(6) (a) Boldyrev, A. I.; Wang, L.-S. *Chem. Rev.* **2005**, *105*, 3716. (b) Tsipis, C. A. *Coord. Chem. Rev.* **2005**, *249*, 2740.

spectroscopic properties of prototypical ligand-stabilized [*cyclo*-$Ru_3(\mu_2\text{-}X)_3]^{0,3+}$ (X = H^-, BH^{2-}, CH_2^-, NH_2^-, OH^-, Cl^-, NH^{2-}, CO, O^{2-}, PH_2^-, CF_2^-, CCl_2^-, CNH^{2-}, N_3^-) isocycles. Why these species are stable molecules and why they exhibit a perfect planar configuration are questions that will attempt to answer herein by means of electronic structure calculation methods at the DFT level of theory. The aromaticity/antiaromaticity of the model [*cyclo*-$Ru_3(\mu_2\text{-}X)_3]^{0,3+}$ isocycles was verified by a number of established criteria of aromaticity. In particular, the nucleus-independent chemical shift, NICS(0), NICS(1), NICS(−1), $NICS_{zz}(1)$, and $NICS_{zz}(-1)$, and the NICS profiles are indicative, except of the parent [*cyclo*-$Ru_3(\mu_2\text{-}X)_3]^{3+}$ molecule, for the aromaticity of the 3-membered ruthenium(II) isocycles. The latter shows a high paratropic response and is characterized as a highly antiaromatic molecule. Along this line, the versatile chemical reactivity of the archetype [*cyclo*-$Ru_3(\mu_2\text{-}H)_3]^{3+}$ molecule related with the activation of small molecules that leads to the breaking of various strong single and double bonds is thoroughly investigated by means of electronic structure computational techniques and the mechanistic details for a representative activation process, that of the dehydrogenation of NH_3 to form an imido-moiety face-capping the Ru_3 ring is presented. Furthermore, the molecular and electronic structures, stabilities, and bonding features of a series of [*cyclo*-$Ru_3(\mu_2\text{-}H)_3(\mu_3\text{-}Nuc)]^{0,1,2+}$ (Nuc = BH, BCN, BOMe, C^{4-}, CH^{3-}, CMe^{3-}, N^{3-}, NH, N_3^-, NCO^-, OCN^-, NCS^-, O^{2-}, S^{2-}, OH^-, P^{3-}, POH^{2-}, Cl^-, O_2^{2-}, NCH, AlMe, GaMe, C_6H_6, and *cyclo*-C_3H_2Me) products formed allowing to react the archetype [*cyclo*-$Ru_3(\mu_2\text{-}H)_3]^{3+}$ molecule with the appropriate substrates are also comprehensibly analyzed.

Computational Details

In view of the good performance of DFT, we were instigated to perform DFT calculations on all stationary points of the potential energy surfaces (PES) we studied using the GAUSSIAN03 program suite.[7] The geometry optimization of the investigated structures was performed in the gas phase at the B3P86 level[8,9] of DFT, using the lanl2dz basis set for the Ru atoms and the 6-31++G(d,p) basis set for the rest of the nonmetal elements (E). We will denote the computational approach used as B3P86/lanl2dz(Ru)∪6-31++G**(E). The choice of the B3P86 functional was based on the more accurate TDB3P86 and magnetic shielding results provided by this functional when compared to the more widely used B3LYP functional.[10] Moreover, the equilibrium geometries of representative ruthenium complexes, which we will discuss later on, obtained from B3P86 are in better agreement with experimental data than those of the B3LYP procedure. In all computations, no constrains were imposed on the geometry. Full geometry optimization was performed for each structure using Schlegel's analytical gradient method,[11] and the attainment of the energy minimum was verified by calculating the vibrational frequencies that result in absence of imaginary eigenvalues. All stationary points have been identified for minimum (number of imaginary frequencies Nimag = 0) or transition states (Nimag = 1). The vibrational modes and the corresponding frequencies are based on a harmonic force field. This was achieved with the SCF convergence on the density matrix of at least 10^{-9} and the rms force less than 10^{-4} au. All bond lengths and bond angles were optimized to better than 0.001 Å and 0.1°, respectively. The computed electronic energies, the enthalpies of reactions, $\Delta_R H_{298}$, and the activation energies, $\Delta G^{\ddagger}_{298}$, were corrected to constant pressure and 298 K for zero point energy (ZPE) differences and for the contributions of the translational, rotational, and vibrational partition functions. For transition states geometry determination, quasi-Newton transit-guided (QSTN) computations were performed.[12]

The natural bond orbital (NBO) population analysis was performed using Weinhold's methodology.[13,14] Percentage compositions of molecular orbitals, Mayer bond orders, and interaction energies (without BSSE corrections) between molecular fragments were calculated using the AOMix program.[15,16] Magnetic shielding tensors have been computed with the GIAO (gauge-including atomic orbitals) DFT method[17,18] as implemented in the GAUSSIAN03 series of programs[7] employing the B3P86 level of theory. Nucleus-independent chemical shifts (NICS) values were computed at the B3P86/lanl2dz(Ru)∪6-31++G**(E) level according to the procedure described by Schleyer et al.[19] The magnetic shielding tensor element was calculated for a ghost atom located at the center of the ring and along the *z*-axis. Negative (diatropic) NICS values indicate aromaticity, whereas positive (paratropic) values imply antiaromaticity.

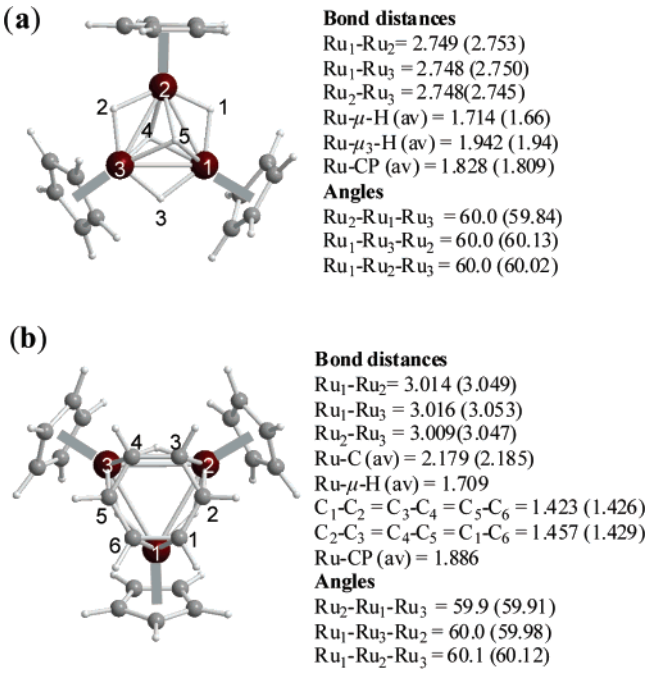

Figure 1. Equilibrium geometries (bond lengths in Å, angles in degrees) of (a) [(η^5-$C_5H_5)_3Ru_3(\mu\text{-}H)_3(\mu_3\text{-}H)_2$] and (b) [($\eta^5$-$C_5H_5)_3Ru_3(\mu\text{-}H)_3(\mu_3\text{-}\eta^2$:$\eta^2$:$\eta^2$-$C_6H_6)$] triruthenium polyhydrido complexes computed at the B3P86 level using the lanl2dz(Ru)∪6-31++G**(E) (E = nonmetal element) basis set. Values in parentheses are selected bond lengths and angles of the [(η^5-$C_5Me_5)_3Ru_3(\mu\text{-}H)_3(\mu_3\text{-}H)_2$] and [($\eta^5$-$C_5Me_5)_3Ru_3(\mu\text{-}H)_3(\mu_3\text{-}\eta^2$:$\eta^2$:$\eta^2$-$C_6H_6)$] complexes determined by X-ray crystallography.

Results and Discussion

Equilibrium Geometries of Representative "Actual" Triruthenium Polyhydrido Complexes. Testing the Performance of the B3P86 Functional. We first tested the perfor-

(7) Frisch, M. J.; et al. *Gaussian 03*, revision B.02; Gaussian, Inc.: Pittsburgh, PA, 2003.
(8) Perdew, J. P. *Phys. Rev. B* **1986**, *33*, 8822.
(9) Becke, A. D. *J. Chem. Phys.* **1993**, *98*, 5648.
(10) Wiberg, K. B.; Stratmann, R. E.; Frisch, M. J. *Chem. Phys. Lett.* **1998**, *297*, 60.
(11) Schlegel, H. B. *J. Comput. Chem.*, **1982**, *3*, 214.
(12) Head-Gordon, M. P.; Frisch, M. J. *Chem. Phys. Lett.* **1988**, *153*, 503−506.
(13) Reed, A. E.; Curtiss, L. A.; Weinhold, F. *Chem. Rev.* **1988**, *88*, 899.
(14) Weinhold, F. In *The Encyclopedia of Computational Chemistry*; Schleyer, P. v. R., Ed.; John Wiley & Sons: Chichester, 1998; pp 1792−1811.
(15) Gorelsky, S. I. *AOMix Program for Molecular Orbital Analysis*; York University: Toronto, Canada (http://www.sg-chem.net).
(16) Gorelsky, S. I.; Lever, A. B. P. *J. Organomet. Chem.* **2001**, *635*, 187.
(17) Ditchfield, R. *Mol. Phys* **1974**, *27*, 789−807.
(18) Gauss, J. *J. Chem. Phys.* **1993**, *99*, 3629.
(19) Schleyer, P. v. R.; Maerker, C.; Dransfeld, A.; Jiao, H.; Hommes, N. J. R. v. E. *J. Am. Chem. Soc.* **1996**, *118*, 6317.

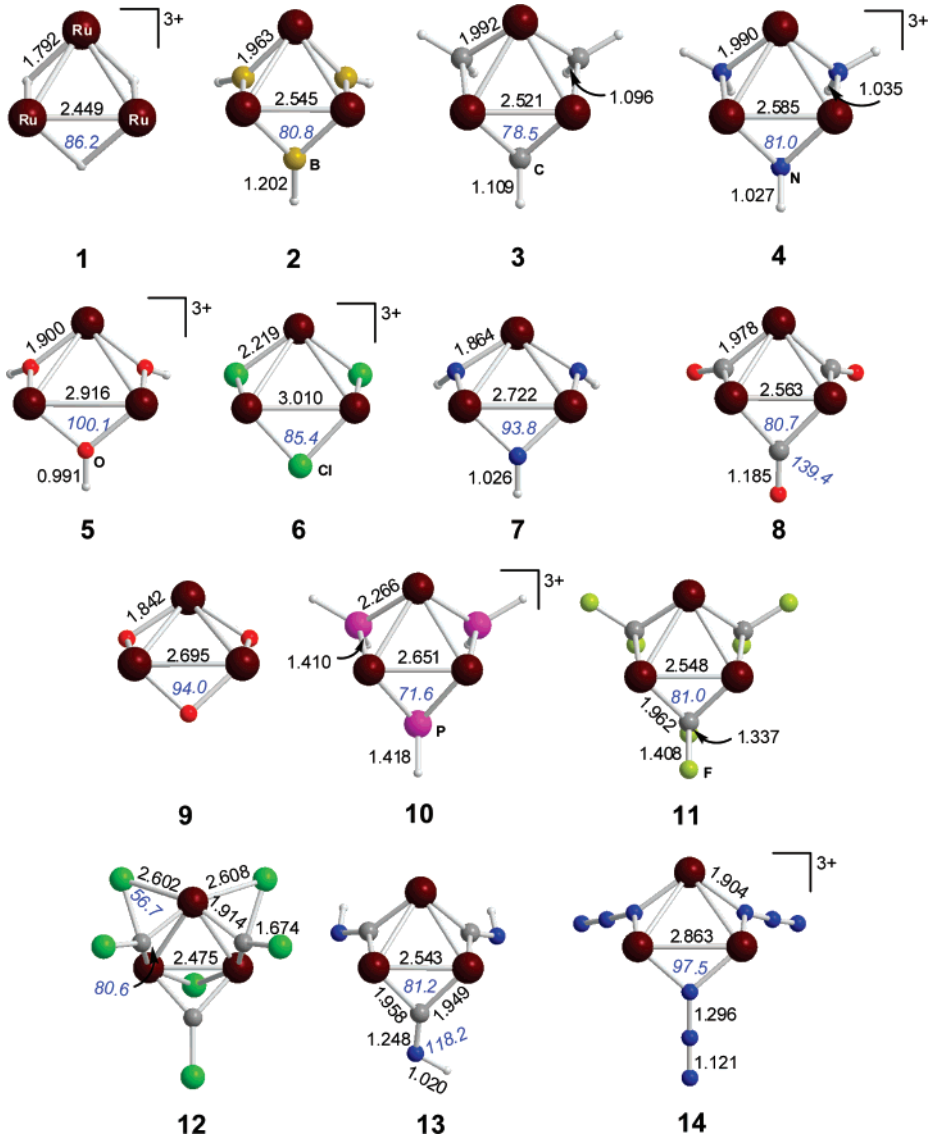

Figure 2. Equilibrium geometries (bond lengths in Å, angles in degrees) of [*cyclo*-$Ru_3(\mu_2\text{-}X)_3]^{0,3+}$ (X = H, BH, CH_2, NH_2, OH, Cl, NH, CO, O, PH_2, CF_2, CCl_2, CNH, N_3) clusters computed at the B3P86/lanl2dz(Ru)∪6-31++G**(E) (E = nonmetal element) level. All [*cyclo*-$Ru_3(\mu_2\text{-}X)_3]^{0,3+}$ molecules, except [*cyclo*-$Ru_3(\mu_2\text{-}Cl)_3(\mu_2\text{-}CCl)_3$], **12**, and [*cyclo*-$Ru_3(\mu_2\text{-}CNH)_3$], **13**, have C_{3v} symmetry. Clusters **12** and **13** belong to C_s and C_1 point groups, respectively.

mance of the B3P86 functional by calculating the equilibrium geometries of two representative "actual" triruthenium polyhydrido complexes (Figure 1). Selected bond lengths and angles of the [(η^5-$C_5Me_5)_3Ru_3(\mu$-H)$_3(\mu_3$-H)$_2$] and [(η^5-$C_5Me_5)_3Ru_3(\mu$-H)$_3(\mu_3$- η^2:η^2:η^2-C_6H_6) complexes determined by X-ray crystallography are also given in Figure 1 (values in parentheses).

Perusal of Figure 1 illustrates the good performance of the B3P86 functional in combination with the lanl2dz(Ru)∪6-31++G**(E) (E = nonmetal element) basis set in reproducing the structures of the [(η^5-$C_5Me_5)_3Ru_3(\mu$-H)$_3(\mu_3$-H)$_2$] and [(η^5-$C_5Me_5)_3Ru_3(\mu$-H)$_3(\mu_3$-η^2:η^2:η^2-C_6H_6) complexes determined by X-ray crystallography. It should be noticed that in the experimental structures the Cp (C_5H_5) ligands are the Cp* (C_5Me_5) ones, thus accounting for the small differences in the Ru−Cp and Ru−Cp* bond lengths observed. In view of the good performance of B3P86/lanl2dz(Ru)∪6-31++G**(E), we were instigated to perform B3P86/lanl2dz(Ru)∪6-31++G**(E) calculations on a series of model unsaturated μ_2-X (X = H, BH, CH_2, NH_2, OH, Cl, NH, CO, O, PH_2, CF_2, CCl_2, CNH, N_3) bridged triruthenium clusters ignoring the Cp or Cp* coligands to asses the stability, diatropicity/paratropicity, and chemical reactivity of the electron-deficient triruthenium ring core structures.

Equilibrium Geometries of Model [*cyclo*-$Ru_3(\mu_2\text{-}X)_3]^{0,3+}$ (X = H, BH, CH_2, NH_2, OH, Cl, NH, CO, O, PH_2, CF_2, CCl_2, CNH, N_3) Triruthenium Clusters. Let us now discuss the most prominent structural features of the [*cyclo*-$Ru_3(\mu_2\text{-}X)_3]^{0,3+}$ (X = H, BH, CH_2, NH_2, OH, Cl, NH, CO, O, PH_2, CF_2, CCl_2, CNH, N_3) triruthenium clusters. Selected bond lengths and angles of the [*cyclo*-$Ru_3(\mu_2\text{-}X)_3]^{0,3+}$ molecules are shown in Figure 2. All [*cyclo*-$Ru_3(\mu_2\text{-}X)_3]^{0,3+}$ molecules, except [*cyclo*-$Ru_3(\mu_2\text{-}Cl)_3(\mu_2\text{-}CCl)_3$], **12**, and [*cyclo*-$Ru_3(\mu_2\text{-}CNH)_3$], **13**, have C_{3v} symmetry. Clusters **12** and **13** belong to C_s and C_1 point groups, respectively.

It can be seen that in all [*cyclo*-$Ru_3(\mu_2\text{-}X)_3]^{0,3+}$ molecules, except cluster **12**, with X = CCl_2, the X ligands bridge symmetrically adjacent ruthenium atoms forming isosceles Ru-(μ-X)Ru triangles that are aligned on the one side of the equilateral Ru_3 triangle forming X−Ru−Ru−Ru dihedral angles in the range of 120.4−142.2°, which follow the trend: NH >

O > N_3 > OH > Cl > CCl > CF_2 > PH_2 > CNH ≈ CO ≈ CH_2 > NH_2 > H > BH. This is exactly the conformation adopted by trinuclear arene ruthenium polyhydrido clusters studied experimentally thus far,[1b,1d,2a,4e] illustrating that the stabilizing cyclopentadiene or benzene coligands do not affect the $Ru_3(\mu_2\text{-}X)_3$ core structure. Noteworthy is the breaking of one of the C−Cl bonds of the CCl_2 bridge, affording μ_2-Cl and μ_2-CCl bridges that are aligned on the opposite sites of the Ru_3 triangle. The high efficiency of the Ru_3 ring in activating and finally breaking the strong C−Cl bonds is then evident.

It is also interesting to be noticed that upon bridging the CH_2, CF_2, NH_2, and PH_2 moieties to the Ru_3 ring the E−H bonds of the EH_2 bridging unit are not equivalent. The E−H bonds aligned toward the center of the ring are shorter than those aligned in the opposite direction by 0.013, 0.071, 0.008, and 0.008 Å for the C−H, C−F, N−H, and P−H bonds, respectively. The shorter C−F bonds are aligned almost perpendicular to the Ru_3 ring plane with the fluorine atoms forming a 3-membered F_3 ring parallel to the Ru_3 ring.

The computed intermetallic Ru···Ru distances found in the range of 2.449−3.010 Å are indicative of metal−metal interactions and follow the trend: $[cyclo\text{-}Ru_3(\mu_2\text{-}H)_3]^{3+}$ < $[cyclo\text{-}Ru_3(\mu_2\text{-}Cl)_3(\mu_2\text{-}CCl)_3]$ < $[cyclo\text{-}Ru_3(\mu_2\text{-}CH_2)_3]$ < $[cyclo\text{-}Ru_3(\mu_2\text{-}CNH)_3]$ ≈ $[cyclo\text{-}Ru_3(\mu_2\text{-}BH)_3]$ ≈ $[cyclo\text{-}Ru_3(\mu_2\text{-}CF_2)_3]$ < $[cyclo\text{-}Ru_3(\mu_2\text{-}CO)_3]$ < $[cyclo\text{-}Ru_3(\mu_2\text{-}NH_2)_3]^{3+}$ < $[cyclo\text{-}Ru_3(\mu_2\text{-}PH_2)_3]^{3+}$ < $[cyclo\text{-}Ru_3(\mu_2\text{-}O)_3]$ < $[cyclo\text{-}Ru_3(\mu_2\text{-}NH)_3]$ < $[cyclo\text{-}Ru_3(\mu_2\text{-}N_3)_3]^{3+}$ < $[cyclo\text{-}Ru_3(\mu_2\text{-}OH)_3]^{3+}$ < $[cyclo\text{-}Ru_3(\mu_2\text{-}Cl)_3]^{3+}$. The Ru−Ru distances are less than those expected by the van der Waals radius for Ru (2.20 Å). The Ru−Ru bond distance in metallic ruthenium is 2.65 Å, whereas in the diatomic Ru_2 molecule it was predicted to be 2.027 Å at the same level of theory. The stronger intermetallic interactions occur in the parent $[cyclo\text{-}Ru_3(\mu_2\text{-}H)_3]^{3+}$ species, and the weaker ones occur in the $[cyclo\text{-}Ru_3(\mu_2\text{-}OH)_3]^{3+}$ and $[cyclo\text{-}Ru_3(\mu_2\text{-}Cl)_3]^{3+}$ clusters. The Ru−X bond lengths in the symmetrical Ru−X−Ru bridges depends on the bridging X ligand following the trend: H < O < NH < OH < N_3 < CCl < CNH ≈ CF_2 ≈ BH < CO < NH_2 ≈ CH_2 < Cl < PH_2.

Stability of the $[cyclo\text{-}Ru_3(\mu_2\text{-}X)_3]^{0,3+}$ (X = H, BH, CH_2, NH_2, OH, Cl, NH, CO, O, PH_2, CF_2, CCl_2, CNH, N_3) Triruthenium Clusters. The stability of the $[cyclo\text{-}Ru_3(\mu_2\text{-}X)_3]^{0,3+}$ (X = H, BH, CH_2, NH_2, OH, Cl, NH, CO, O, PH_2, CF_2, CCl_2, CNH, N_3) molecules are investigated using the following fragmentation schemes:

$$[cyclo\text{-}Ru_3(\mu_2\text{-}X)_3]^{0,3+} \rightarrow 3[RuX]^{0,1+}$$

$$[cyclo\text{-}Ru_3(\mu_2\text{-}X)_3]^{0,3+} \rightarrow 3Ru^{2+} + 3[X]^{1-,2-}$$

The calculated binding energies are compiled in Table 1.

It can be seen that all $[cyclo\text{-}Ru_3(\mu_2\text{-}X)_3]^{0,3+}$ molecules are predicted to be bound with respect to their dissociation to "free" Ru^{2+} and $[X]^{0,1-,2-}$ moieties in their ground states. The stabilization of the $[cyclo\text{-}Ru_3(\mu_2\text{-}X)_3]^{0,3+}$ species with respect to the free Ru^{2+} and $[X]^{0,1-,2-}$ moieties follows the trend: **9** > **7** > **2** > **3** > **11** > **13** > **12** > **8** > **6** > **4** > **10** > **5** > **1** > **14**. Notably, the clusters **6**, **4**, **10**, **5**, **1**, and **14** involving the chloride, amido, phoshido, hydroxide, hydrido, and azido-bridges, respectively, are much less stabilized relative to the rest of the tiruthenium clusters. These cationic clusters are predicted to be unbound with respect to dissociation to the $[RuX]^+$ monomeric species, whereas the remaining clusters, all being neutral, are predicted to be bound. The stabilization of the latter follows the trend: **9** > **12** > **2** > **7** > **3** > **11** > **13** > **8**. It should be noticed that cluster **12** exhibits a different structural core involving a total of six bridges, three Cl^- and three CCl^- bridges.

Table 1. Binding Energies ΔE_1 and ΔE_2 (in kcal mol^{-1}) of the $[cyclo\text{-}Ru_3(\mu_2\text{-}X)_3]^{0,3+}$ (X = H, BH, CH_2, NH_2, OH, Cl, NH, CO, O, PH_2, CF_2, CCl_2, CNH, N_3) Clusters Computed at the B3P86/lanl2dz(Ru)∪6-31++G**(E) (*E* = Nonmetal Element) Basis Set

cluster	ΔE_1[a]	ΔE_1/mol $[RuX]^{0,1+,2+}$	ΔE_2[b]
$[cyclo\text{-}Ru_3(\mu_2\text{-}H)_3]^{3+}$, **1**	176.6	58.9	−1208.0
$[cyclo\text{-}Ru_3(\mu_2\text{-}BH)_3]$, **2**	−237.6	−79.2	−2717.2
$[cyclo\text{-}Ru_3(\mu_2\text{-}CH_2)_3]$, **3**	−210.8	−70.3	−2683.5
$[cyclo\text{-}Ru_3(\mu_2\text{-}NH_2)_3]^{3+}$, **4**	66.7	22.2	−1418.8
$[cyclo\text{-}Ru_3(\mu_2\text{-}OH)_3]^{3+}$, **5**	93.5	31.2	−1275.1
$[cyclo\text{-}Ru_3(\mu_2\text{-}Cl)_3]^{3+}$, **6**	89.8	29.9	−1661.1
$[cyclo\text{-}Ru_3(\mu_2\text{-}NH)_3]$, **7**	−221.1	−73.7	−2744.4
$[cyclo\text{-}Ru_3(\mu_2\text{-}CO)_3]$, **8**	−171.2	−57.1	−2229.3
$[cyclo\text{-}Ru_3(\mu_2\text{-}O)_3]$, **9**	−243.3	−81.1	−2748.6
$[cyclo\text{-}Ru_3(\mu_2\text{-}PH_2)_3]^{3+}$, **10**	1.7	0.6	−1373.3
$[cyclo\text{-}Ru_3(\mu_2\text{-}CF_2)_3]$, **11**	−201.6	−67.2	−2658.0
$[cyclo\text{-}Ru_3(\mu_2\text{-}Cl)_3(\mu_2\text{-}CCl)_3]$, **12**	−242.9	−81.0	−2308.0
$[cyclo\text{-}Ru_3(\mu_2\text{-}CNH)_3]$, **13**	−187.8	−62.6	−2558.7
$[cyclo\text{-}Ru_3(\mu_2\text{-}N_3)_3]^{3+}$, **14**	49.6	16.5	−1201.2

[a] $\Delta E_1 = E([cyclo\text{-}Ru_3(\mu_2\text{-}X)_3]^{0,3+}) - [3E(RuX^{0,1+}]$. [b] $\Delta E_2 = E([cyclo\text{-}Ru_3(\mu_2\text{-}X)_3]^{0,3+}) - [3E(Ru^{2+}) + 3E(X^{1-,2-})]$.

Electronic and Bonding Properties of the $[cyclo\text{-}Ru_3(\mu_2\text{-}X)_3]^{0,3+}$ (X = H, BH, CH_2, NH_2, OH, Cl, NH, CO, O, PH_2, CF_2, CCl_2, CNH, N_3) Triruthenium Clusters. To understand the structural integrity of the $[cyclo\text{-}Ru_3(\mu_2\text{-}X)_3]^{0,3+}$ (X = H, BH, CH_2, NH_2, OH, Cl, NH, CO, O, PH_2, CF_2, CCl_2, CNH, N_3) molecules, their valence molecular orbitals, shown in Scheme 2, have been analyzed. The bonding in the 3-membered ruthenium rings is characterized by a common ring-shaped electron density, more commonly seen in aromatic organic molecules and in "all-metal" aromatics.[6]

The lowest unoccupied molecular orbitals (LUMOs) of all cationic 3-membered ruthenium isocycles correspond to π^* antibonding combination of 4d (Ru) orbitals. The nature of the LUMO suggests that nucleophiles would attack the Ru_3 ring over its centroid in line with experimental observation, which will be discussed latter on. On the other hand, the LUMO of the neutral 3-membered ruthenium isocycles corresponds to σ^* antibonding combination of 4d (Ru) orbitals, and therefore, nucleophiles would attack the Ru corners along the Ru_3 ring plane.

Perusal of Scheme 2 reveals that the Ru_3 ring structural core exhibits a composite bonding mode involving σ-, π-, and δ-type MOs. Noteworthy is the presence of π-type MOs resulting from the bonding interaction of the 4d AOs of the Ru atoms, delocalized over the entire metallic framework analogous to the π-type MOs of the aromatic cyclopropenium cation, which support a ring current. However, there is a striking difference in the shape of the cyclic delocalized electron density of the aromatic cyclopropenium cation compare to the Ru_3 isocycles, owing to the alignment of the bridging ligands X on the one side of the Ru_3 plane forming a triangle parallel to the Ru_3 triangle in a staggered conformation. Such an alignment perturbs the cyclic electron cloud on the two sides of the Ru_3 ring by distending the electron cloud found in the opposite side. Therefore, the cyclic delocalizations on the two sides of the Ru_3 ring are not equivalent (see the HOMO-4 and HOMO-8 of

Scheme 2. Most Relevant Valence Molecular Orbitals of [*cyclo*-$Ru_3(\mu_2\text{-}H)_3]^{3+}$, **1**, [*cyclo*-$Ru_3(\mu_2\text{-}BH)_3$], **2**, -[*cyclo*-$Ru_3(\mu_2\text{-}CO)_3$], **8**, and [*cyclo*-$Ru_3(\mu_2\text{-}N_3)_3]^{3+}$, **14**

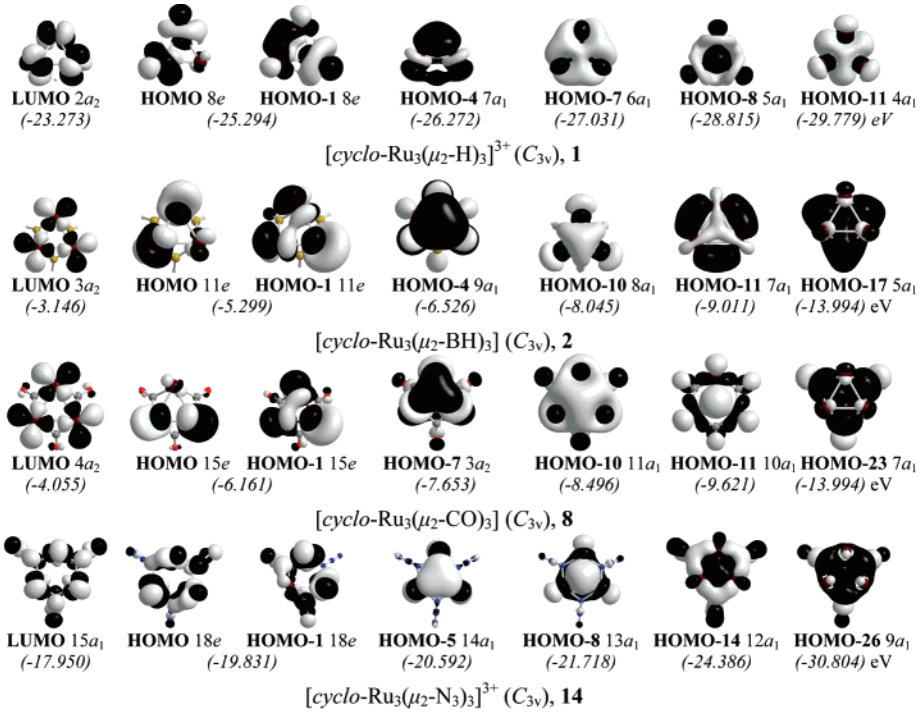

1, HOMO-4 and HOMO-10 of **2**, HOMO-7 and HOMO-11 of **8** and HOMO-5, HOMO-8, and HOMO-14 of **14** in Scheme 2), and consequently, the induced ring currents on each side of the Ru_3 ring would be different, as is shown later on. This is the first example of aromatic systems exhibiting different aromaticity on the two sides of the aromatic ring, e.g., above and below the geometrical center of the ring. The delocalized σ- and π-electron density in the Ru_3 rings could probably account for the observed equivalence of the Ru−Ru bonds. R. B. King[20] proposed a bonding model in M_3 (M = Fe, Ru, Os) triangles of the $M_3(CO)_{12}$ metal carbonyl clusters based on the concept of σ-aromaticity, which partitions the six orbitals and six electrons available for bonding within the M_3 triangle into a core 3c-2e bond of Hückel topology formed by radial hybrid orbitals and a surface 3c-4e bond of Möbius topology formed by tangential p orbitals. In effect, such orbitals exist in the Ru_3 ring structural cores under consideration. More recently, R. B. King et al.[21] provided the first quantitative evidence for the σ-aromatic nature of the $[M_3(CO)_{12}]$ (M = Fe, Ru, Os) species based on structural and nucleus-independent chemical-shift analysis.

Selected electronic parameters of the 3-membered ruthenium ring structural cores have been collected in Table 2.

The stability of the triangular Ru_3 structural cores is reflected on the $\epsilon_{LUMO} - \epsilon_{HOMO}$ energy gap, the so-called global hardness η. According to the computed η values and the principle of maximum hardness,[22] cluster **12** is the most stable in the series, because it involves a total of six bridges between the Ru atoms, three Cl^- and three CCl^- bridges.

According to the Natural bond orbital (NBO) population analysis (Table 2), there is a strong charge transfer of natural charge from the bridging ligands to Ru(II) metal atoms amounted to 0.85−2.09 |e|. The highest charge transfer occurs in the μ_2-BH bridged cluster, **2**, and the lowest one in the μ_2-OH cluster, **5**. The transferred electron density is accumulated on the vacant 4d and 5s orbitals of the Ru(II) metal centers, which acquire a natural electron configuration $4d^{6.69-7.74}5s^{0.15-0.39}$ (Table 2). Finally, the electron deficiency of the Ru_3 ring renders the [*cyclo*-$Ru_3(\mu_2\text{-}X)_3]^{0,3+}$ clusters strongly electrophilic, particularly the positively charged ones having a high electrophilicity index[23] in the range of 85.3−145.9, capable to interact with a variety of nucleophiles, as will be discussed later on.

Table 2. Selected Electronic Parameters of the 3-Membered Ruthenium Ring Structural Cores Computed at the B3P86/lanl2dz(Ru)∪6-31++G**(E) (*E* = Nonmetal Element) Level

cluster	E_{HOMO}	E_{LUMO}	η	ω^a	*nec*(Ru)[b] 4*d*/5*s*	q_{Ru}
1	−25.294	−23.273	2.021	145.9	6.74/0.30	0.93
2	−5.299	−3.146	2.153	4.1	7.74/0.39	−0.09
3	−5.048	−2.905	2.143	3.7	7.40/0.38	0.24
4	−21.448	−19.092	2.356	87.2	6.85/0.22	0.92
5	−21.845	−19.831	2.014	107.8	6.69/0.15	1.15
6	−22.383	−20.723	1.660	139.9	7.00/0.19	0.77
7	−5.160	−3.217	1.943	4.5	7.28/0.30	0.42
8	−6.161	−4.055	2.106	6.2	7.55/0.33	0.13
9	−5.897	−4.220	1.677	7.8	7.08/0.25	0.65
10	−20.422	−18.232	2.190	85.3	7.39/0.27	0.31
11	−6.235	−3.990	2.245	5.8	7.48/0.36	0.18
12	−7.717	−5.348	2.369	9.0	7.24/0.28	0.48
13	−5.609	−3.512	2.097	5.0	7.52/0.33	0.18
14	−19.831	−17.950	1.881	94.9	6.94/0.19	0.88

[a] Electrophilicity index $\omega = \mu^2/2\eta$, where μ and η are the chemical potential and hardness, respectively, given approximately by the expressions $\mu = (\epsilon_{LUMO} + \epsilon_{HOMO})/2$ and $\eta = (\epsilon_{LUMO} - \epsilon_{HOMO})$. ϵ_{HOMO}, ϵ_{LUMO}, η and ω are given in eV. [b] Natural electron configuration (*nec*).

NMR Spectra and Aromaticity/Antiaromaticity of the [*cyclo*-$Ru_3(\mu_2\text{-}X)_3]^{0,3+}$ (X = H, BH, CH_2, NH_2, OH, Cl, NH, CO, O, PH_2, CF_2, CCl_2, CNH, N_3) Triruthenium Clusters.

(20) King, R. B. *Inorg. Chim. Acta* **2003**, *350*, 126.
(21) Corminboeuf, C.; Schleyer, P. v. R.; King, R. B. *Chem.−Eur. J.* **2007**, *13*, 978.
(22) Parr, R. G.; Chattaraj, P. K. *J. Am. Chem. Soc.* **1991**, *113*, 1854.
(23) Parr, R. G. v.; Szentpaly, L.; Liu, S. *J. Am. Chem. Soc.* **1999**, *121*, 1922.

Table 3. NICS Values (in ppm) Calculated at the Ring Center, NICS(0), 1.0 Å Above and Below the Ring Center, NICS(1) and NICS(−1), Respectively, and the zz-Component of the Shielding Tensor Element, $NICS_{zz}(1)$ and $NICS_{zz}(-1)$ along with the Distance between the Centroids of the Ru_3 and X_3 Ring Planes (in Å) for the [*cyclo*-$Ru_3(\mu_2\text{-}X)_3]^{0,3+}$ Clusters Computed at the GIAO/B3P86/lanl2dz(Ru)∪6-31++G**(E) (*E* = Nonmetal Element) Level

cluster	NICS(0)	NICS(1)	NICS(−1)	$NICS_{zz}(1)$	$NICS_{zz}(-1)$	$R(Ru_3\cdots X_3)$
[*cyclo*-$Ru_3(\mu_2\text{-}H)_3]^{3+}$, **1**	1032.8	299.8	222.3	−104.3	26.3	1.130
[*cyclo*-$Ru_3(\mu_2\text{-}BH)_3$], **2**	−35.1	−4.4	−21.9	−10.7	−33.8	1.315
[*cyclo*-$Ru_3(\mu_2\text{-}CH_2)_3$], **3**	−43.5	6.4	−40.7	−8.7	−25.9	1.260
[*cyclo*-$Ru_3(\mu_2\text{-}NH_2)_3]^{3+}$, **4**	−52.5	15.6	−46.4	−1.9	−31.8	1.244
[*cyclo*-$Ru_3(\mu_2\text{-}OH)_3]^{3+}$, **5**	−80.3	−47.0	−29.0	−72.5	−75.7	0.847
[*cyclo*-$Ru_3(\mu_2\text{-}Cl)_3]^{3+}$, **6**	−131.9	−92.8	−4.5	−208.0	3.4	1.180
[*cyclo*-$Ru_3(\mu_2\text{-}NH)_3$], **7**	−100.0	−34.8	−57.5	−38.0	−99.6	0.748
[*cyclo*-$Ru_3(\mu_2\text{-}CO)_3$], **8**	−32.9	5.1	−30.2	−6.5	−40.6	1.216
[*cyclo*-$Ru_3(\mu_2\text{-}O)_3$], **9**	−82.9	−17.8	−69.1	−7.6	−122.0	0.767
[*cyclo*-$Ru_3(\mu_2\text{-}PH_2)_3]^{3+}$, **10**	−53.2	9.0	−46.0	−1.2	−23.5	1.477
[*cyclo*-$Ru_3(\mu_2\text{-}CF_2)_3$], **11**	−38.3	5.8	−31.5	−3.1	−32.6	1.173
[*cyclo*-$Ru_3(\mu_2\text{-}Cl)_3(\mu\text{-}CCl)_3$], **12**	−50.2	−3.1	−21.4	9.0	−28.3	1.655;1.131
[*cyclo*-$Ru_3(\mu_2\text{-}CNH)_3$], **13**	−34.5	6.0	−33.0	−4.7	−37.9	1.218
[*cyclo*-$Ru_3(\mu_2\text{-}N_3)_3]^{3+}$, **14**	−95.9	−35.9	−44.7	−49.6	−90.0	0.838
[*cyclo*-$Ru_3(\mu_2\text{-}H)_3]^{+}$	−489.6	−180.2	−336.6	−161.5	19.0	1.004

Planarity, high stability, bond length equalization, and hardness are conventionally good indicators of aromaticity, but this is restrictive in many examples. At present, the NICS, proposed by Schleyer and co-workers,[19] is an efficient and simple criterion in probing the aromaticity/antiaromaticity of a molecule, which is based on the negative of the magnetic shielding computed, for example, at or above the geometrical centers of rings or clusters. Systems with negative NICS values are aromatic, and systems with strongly positive NICS values are antiaromatic. The computed NICS values at the geometrical centers of the Ru_3 rings, NICS(0), 1.0 Å above, NICS(1), and below the ring center, NICS(−1), and the zz-component of the shielding tensor element, $NICS_{zz}(1)$ and $NICS_{zz}(-1)$, are compiled in Table 3.

The conspicuous feature of the results given in Table 3 is that the [*cyclo*-$Ru_3(\mu\text{-}H)_3]^{3+}$, **1**, molecule is uniquely antiaromatic whereas all of the other molecules are aromatic. The fundamental issue of the different behavior of the [*cyclo*-$Ru_3(\mu\text{-}H)_3]^{3+}$ molecule could be understood by considering the total number of valence electrons of the [*cyclo*-$Ru_3(\mu_2\text{-}X)_3]^{0,3+}$ clusters. Notice that the hydride ligand with $1s^2$ electron configuration acts as a two-electron donor in the formation of the Ru−H−Ru hydride bridges, whereas all of the other X donor atoms (X = B, C, N, O, S, P, Cl) having filled p orbitals and, as well, can act as donors of two electron pairs to the bridging Ru atoms in the formation of the Ru−X−Ru bonds.

The parent [*cyclo*-$Ru_3(\mu\text{-}H)_3]^{3+}$, **1**, species is a highly unsaturated 24 valence electron (24e) species that conforms to the Hückel rule of antiaromaticity (4n electrons); thereby, it is expected to be a highly antiaromatic system. The same holds also true for the [*cyclo*-$Ru_3(\mu\text{-}Cl)_3(\mu\text{-}CCl)_3$], **12**, species, which is a 48e system. Indeed, applying the magnetic criterion of aromaticity, viz. NICS, we were able to diagnose a high paratropic response for **1**, which is quantified by the NICS(0), NICS(1), and NICS(−1) values of 1032.8, 299.8, and 222.3 ppm, respectively. For cluster **12**, although the NICS(0) value is indicative of diatropicity at the center of the ring, the positive $NICS_{zz}(1)$ value illustrates the antiaromatic character of **12**. The rest of the [*cyclo*-$Ru_3(\mu_2\text{-}X)_3]^{0,3+}$ clusters are unsaturated 30 valence electron (30e) species that conform to the Hückel rule of aromaticity (4n + 2 electrons), thereby, they are expected to be aromatic systems. In effect, the NICS(0) and $NICS_{zz}(1)$ values are in support of the aromaticity of these species. However, for clusters **3**, **4**, **8**, **10**, **11**, and **13**, the positive NICS(1) values are compatible with paratropicity of the one side of the Ru_3 ring, but the negative NICS(−1) and $NICS_{zz}(1)$ values are in support of diatropicity on the side where the bridging ligands X reside.

Adding two electrons on the highly antiaromatic [*cyclo*-$Ru_3(\mu\text{-}H)_3]^{3+}$, **1**, species, the resulting [*cyclo*-$Ru_3(\mu\text{-}H)_3]^{+}$ molecule is a 26 valence electron (26e) system conforming to the Hückel rule of aromaticity; thereby, it is expected to be a strongly aromatic molecule. In effect, the NICS(0), NICS(1), and NICSzz(1) values of −489.6, −180.2, and −161.5 ppm (Table 3), respectively, illustrate the high aromaticity of the [*cyclo*-$Ru_3(\mu\text{-}H)_3]^{+}$ species. The addition of two electrons in the [*cyclo*-$Ru_3(\mu\text{-}H)_3]^{3+}$, **1**, species enlarges the equilateral Ru_3 triangle (Ru−Ru bond length of 2.509 Å), shortens the Ru−H bond distances (Ru−H bond lengths of 1.752 Å), and opens the Ru−H−Ru bond angle (Ru−H−Ru bond angle opens by 5.2°).

To get a better insight into the origin of the aromaticity/antiaromaticity of the [*cyclo*-$Ru_3(\mu_2\text{-}X)_3]^{0,3+}$ rings, we applied the recently proposed NICS scan procedure, which is based on scanning the NICS, σ(bq), values over a distance *R* and dissecting them into in-plane, $\sigma(bq_{in})$, and out-of-plane, $\sigma^{zz}(bq_{out})$, components.[24,25] The NICS scan pictures for the isotropic out-of-plane, $\sigma^{iso}(bq_{out})$, in-plane, $\sigma(bq_{in})$, and $\sigma^{zz}(bq_{out})$ tensors of representative clusters **1**, **2**, **8**, and **14** are given in Figure 3. Analogous are the $\sigma(bq)/R(bq)$ curves for the rest of the [*cyclo*-$Ru_3(\mu_2\text{-}X)_3]^{0,3+}$ clusters (Figure S1).

The NICS scan pictures clearly shows the dramatic change of the aromaticity/antiaromaticity on the two sides of the Ru_3 ring. This change could be explained on the grounds of the different coordination environment above and below the Ru_3 ring. In all [*cyclo*-$Ru_3(\mu_2\text{-}X)_3]^{0,3+}$ species, the bridging X ligands form a X_3 triangle parallel to the Ru_3 triangle at distances ranging from 0.748 up to 1.655 Å. C···C interactions between the axial CO ligands in the $Ru_3(CO)_{12}$ cluster resulting in the formation of C_3 triangular ring parallel to the Ru_3 ring have been identified by experimental charge density determination.[26] The valence orbitals localized on the X_3 triangle strongly perturbs the cyclic delocalized electron density on the Ru_3

(24) (a) Stanger, A. *J. Org. Chem.* **2006**, *71*, 883. (b) Stanger, A. *Chem.−Eur. J.* **2006**, *12*, 2745.
(25) (a) Poater, J.; Bofill, J. M.; Alemany, P.; Solà, M. *J. Org. Chem.* **2006**, *71*, 1700. (b) Jiménez-Halla, J. O. C.; Matito, E;. Robles, J.; Solà, M. *J. Organometal. Chem.* **2006**, *691*, 4359.
(26) Gervasio, G.; Bianchi, R.; Marabello, D. *Chem. Phys. Lett.* **2005**, *407*, 18.

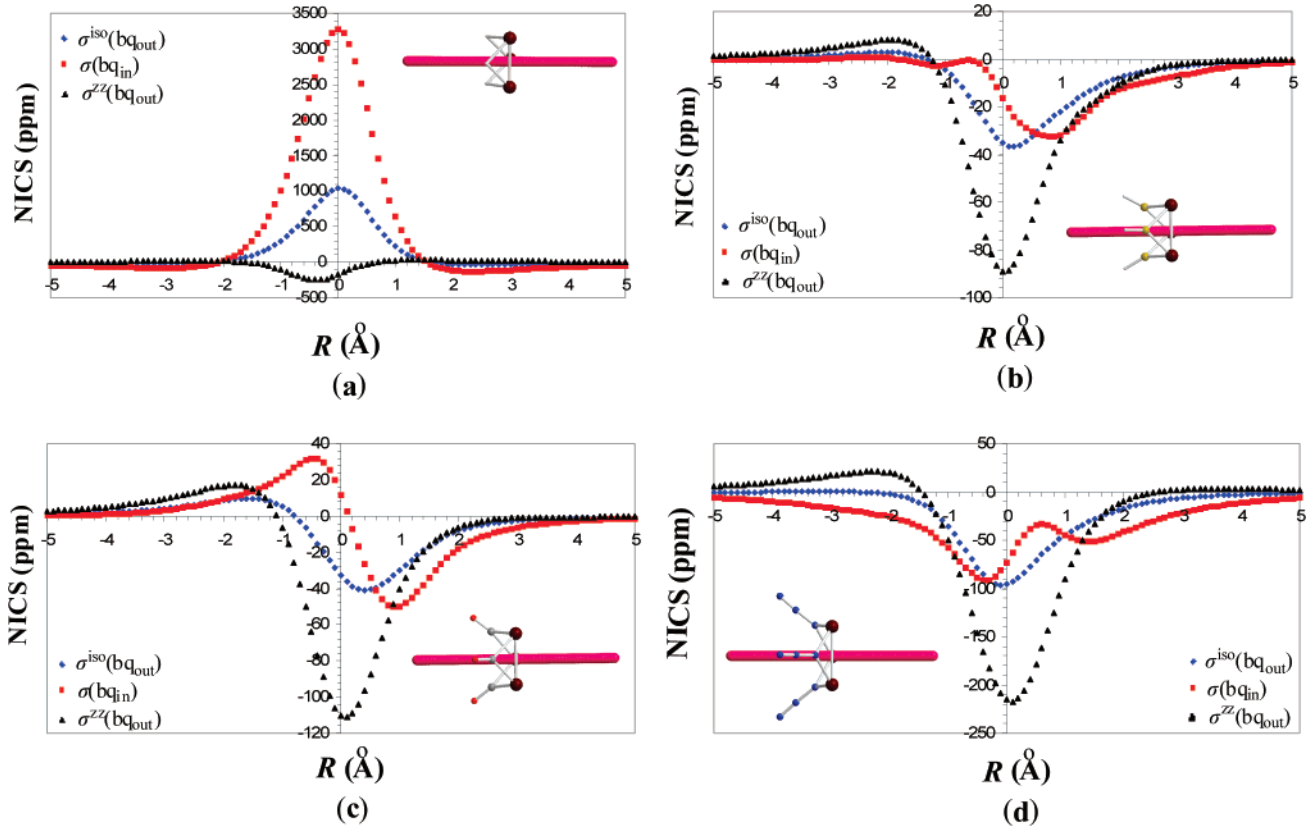

Figure 3. NICS scan pictures for the isotropic out-of-plane, $\sigma^{iso}(bq_{out})$, the in-plane, $\sigma(bq_{in})$, and the out-of-plane, $\sigma^{zz}(bq_{out})$, tensors of the (a) [*cyclo*-$Ru_3(\mu_2\text{-H})_3]^{3+}$, **1**, (b) [*cyclo*-$Ru_3(\mu_2\text{-BH})_3$], **2**, (c) [*cyclo*-$Ru_3(\mu_2\text{-CO})_3$], **8**, and (d) [*cyclo*-$Ru_3(\mu_2\text{-N}_3)_3]^{3+}$, **14**, molecules.

triangle so that it is pushed out from the Ru_3 triangle in the opposite side. Moreover, the diatropicity/paratropicity at the center of the X_3 ring contributes to the diatropicity/paratropicity of the Ru_3 ring at the point −1 Å distant from the geometrical center of the ring, which is very close to the geometrical center of the X_3 ring.

The high antiaromatic character of the parent [*cyclo*-$Ru_3(\mu\text{-H})_3]^{3+}$, **1**, accounts well for the peculiar reaction field of the triruthenium ring core structures. Upon coordination of cyclopentadiene ligands to Ru(II) metal centers to obtain an "actual" $[Cp_3Ru_3(\mu\text{-H})_3]$ cluster, the antiaromatic character is dramatically diminished, corresponding to NICS(0), NICS(1), and $NICS_{zz}(1)$ values of −3.1, 30.0, and 138.4 ppm, respectively. These data were obtained through calculations on the structure of the "actual" $[Cp_3Ru_3(\mu\text{-H})_3(\mu_3\text{-H})_2]$ after eliminating the two μ_3-H ligands, since all attempts to calculate the equilibrium structure of the $[Cp_3Ru_3(\mu\text{-H})_3]$ species did not converged to a minimum. The antiaromatic [*cyclo*-$Ru_3(\mu\text{-H})_3]^{3+}$, **1**, catalyzes the selective activation of B−H, C−H, N−H, O−H, S−H, H−H, C−C, and C═C bonds, and the hydrogenation of aromatics and strongly interacts with a variety of nucleophiles Nuc yielding face-capped [*cyclo*-$Ru_3(\mu\text{-H})_3(\mu_3\text{-Nuc})]^q$ ($q = -1$, 0, +1, +2) clusters involving the capping ligand in a μ_3-Nuc coordination mode. The structural, energetic, and electronic properties of the [*cyclo*-$Ru_3(\mu\text{-H})_3(\mu_3\text{-Nuc})]^q$, ($q = -1$, 0, +1, +2) clusters are discussed in the following section.

Equilibrium Geometries of [*cyclo*-$Ru_3(\mu\text{-H})_3(\mu_3\text{-Nuc})]^q$ (Nuc = BH, BCN, BOMe, C^{4-}, CH^{3-}, CMe^{3-}, N^{3-}, NH, N_3^-, OCN^-, SCN^-, O^{2-}, S^{2-}, OH^-, P^{3-}, POH^{2-}, Cl^-, O_2^{2-}, HCN, AlMe, GaMe; $q = -1$, 0, +1, +2, +3) Clusters. Let us now discuss the most prominent structural features of the *cyclo*-[$Ru_3(\mu\text{-H})_3(\mu_3\text{-Nuc})]^q$ (Nuc = BH, **15**, BCN, **16**, BOMe, **17**, C^{4-}, **18**, CH^{3-}, **19**, CMe^{3-}, **20**, N^{3-}, **21**, NH, **22**, N_3^-, **23**, NCO^-, **24**, OCN^-, **25**, NCS^-, **26**, O^{2-}, **27**, S^{2-}, **28**, OH^-, **29**, P^{3-}, **30**, POH^{2-}, **31**, Cl^-, **32**, O_2^{2-}, **33**, HCN, **34**, AlMe, **35**, GaMe, **36**; $q = -1$, 0, +1, +2, +3) clusters. Selected bond lengths and angles of the [*cyclo*-$Ru_3(\mu\text{-H})_3(\mu_3\text{-Nuc})]^q$ molecules computed at the B3P86/lanl2dz(Ru)∪6-31++G**(E) (*E* = nonmetal element) level are shown in Figures 4 and 5.

It can be seen that in all [*cyclo*-$Ru_3(\mu\text{-H})_3(\mu_3\text{-Nuc})]^q$ molecules, except clusters **35** and **36**, the nucleophile Nuc is coordinated to Ru_3 ring in a μ_3-Nuc coordination mode capping the face of the ring from the most antiaromatic side, which is the side opposite to that of the bridging hydride ligands. This is exactly the case of "actual" $[(\eta^5\text{-}C_5Me_5)_3Ru_3(\mu\text{-H})_3(\mu_3\text{-Nuc})]^q$ and $[(\eta^6\text{-}C_6Me_6)_2(\eta^6\text{-}C_6H_6)Ru_3(\mu\text{-Nuc})]^q$ molecules that have been extensively studied experimentally.[1,2]

[*cyclo*-$Ru_3(\mu\text{-H})_3(\mu_3\text{-BH})]^+$, **15**, [*cyclo*-$Ru_3(\mu\text{-H})_3(\mu_3\text{-BCN})]^+$, **16**, [*cyclo*-$Ru_3(\mu\text{-H})_3(\mu_3\text{-BOMe})]^+$, **17**, comprise the core structure of the "actual" single-faced μ_3-borylene $[(\eta^5\text{-}C_5Me_5)_3Ru_3(\mu\text{-H})_3(\mu_3\text{-BX})]^+$ clusters obtained upon reacting the cationic hexalyhydride $[(\eta^5\text{-}C_5Me_5)_3Ru_3(\mu\text{-H})_6]^+$ cluster with an equimolar amount of $NaBH_4$ or $NaB(CN)H_3$ at room temperature.[1g] Upon coordination of the borylene ligand, the equilateral Ru_3 triangle becomes an isosceles triangle with one short and two longer sides. The average Ru−B distances of 2.050, 2.090, and 2.102 Å for **15**, **16**, and **17**, respectively, lie in the range of

(27) (a) Braunschweig, H. *Angew. Chem., Int. Ed.* **1998**, *37*, 1786 and references therein. (b) Braunschweig, H.; Colling, M. *J. Organometal. Chem.* **2000**, *614*−*615*, 18.

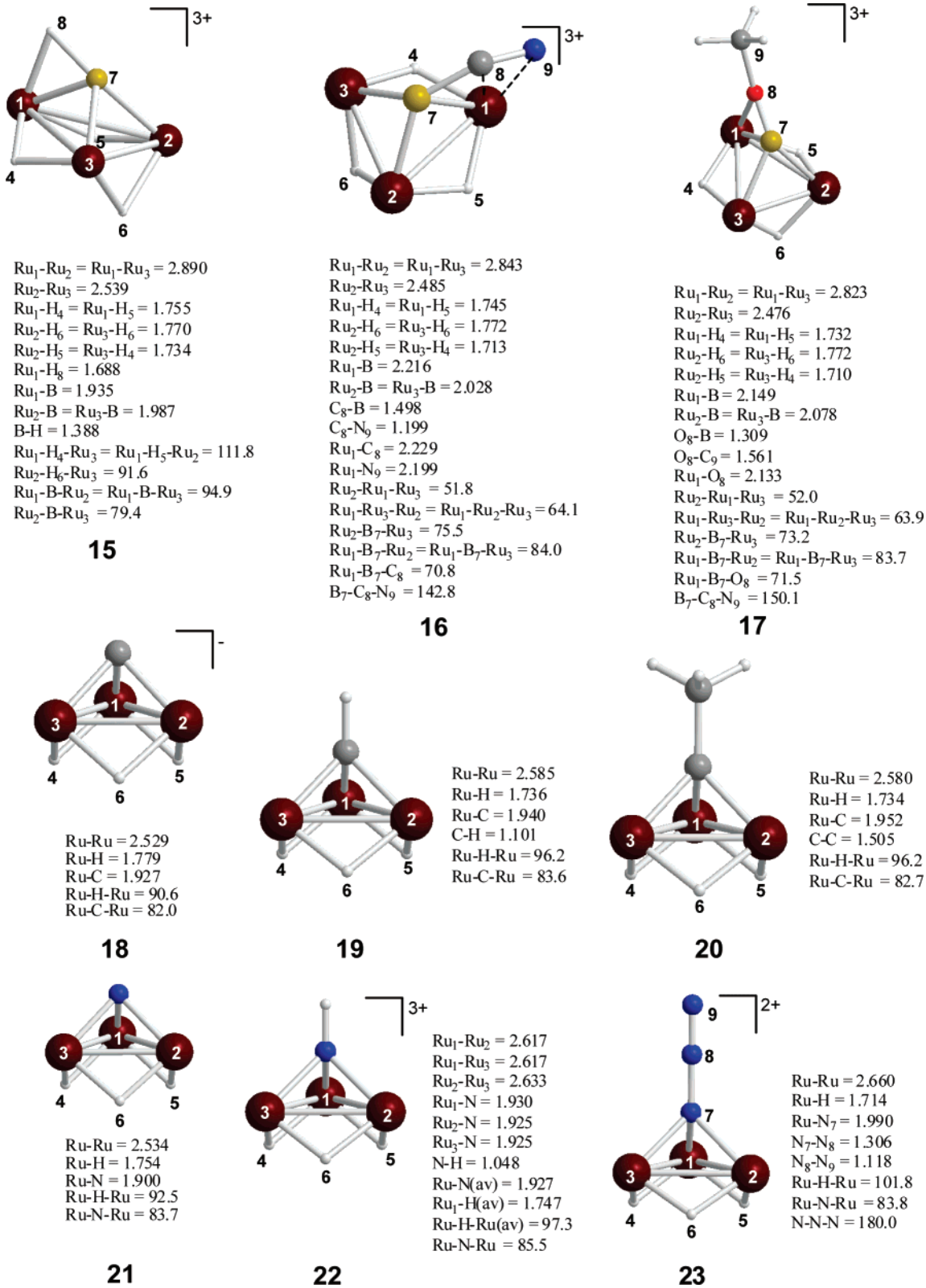

Figure 4. Equilibrium geometries (bond lengths in Å, angles in degrees) of [*cyclo*-$Ru_3(\mu\text{-H})_3(\mu_3\text{-Nuc})]^q$ (Nuc = BH, **15**, BCN, **16**, BOMe, **17**, C^{4-}, **18**, CH^{3-}, **19**, CMe^{3-}, **20**, N^{3-}, **21**, NH, **22**, and N_3^-, **23**; $q = -1, 0, +1$) clusters computed at the B3P86/lanl2dz(Ru)∪6-31++G**(E) (E = nonmetal element) level.

those reported for the transition metal borylene complexes.[27] The average Ru−B distance in the "actual" $[(\eta^5\text{-}C_5Me_5)_3Ru_3(\mu\text{-H})_3(\mu_3\text{-BOMe})]^+$ cluster is 2.154 Å. In cluster **16**, the cyanide moiety is aligned in such a way as to favor κ^2-C,N coordination with one of the Ru(II) metal centers as well. Similarly, in cluster **17**, the triply bridged BOMe ligand is also coordinated to a Ru(II) metal center via the O-donor atom.

Clusters **18**, **19**, and **20** consist of an equilateral triangular cluster of three Ru(II) atoms with triply bridging tetraanionic carbon, carbyne, and methylcarbyne ligands, respectively. The

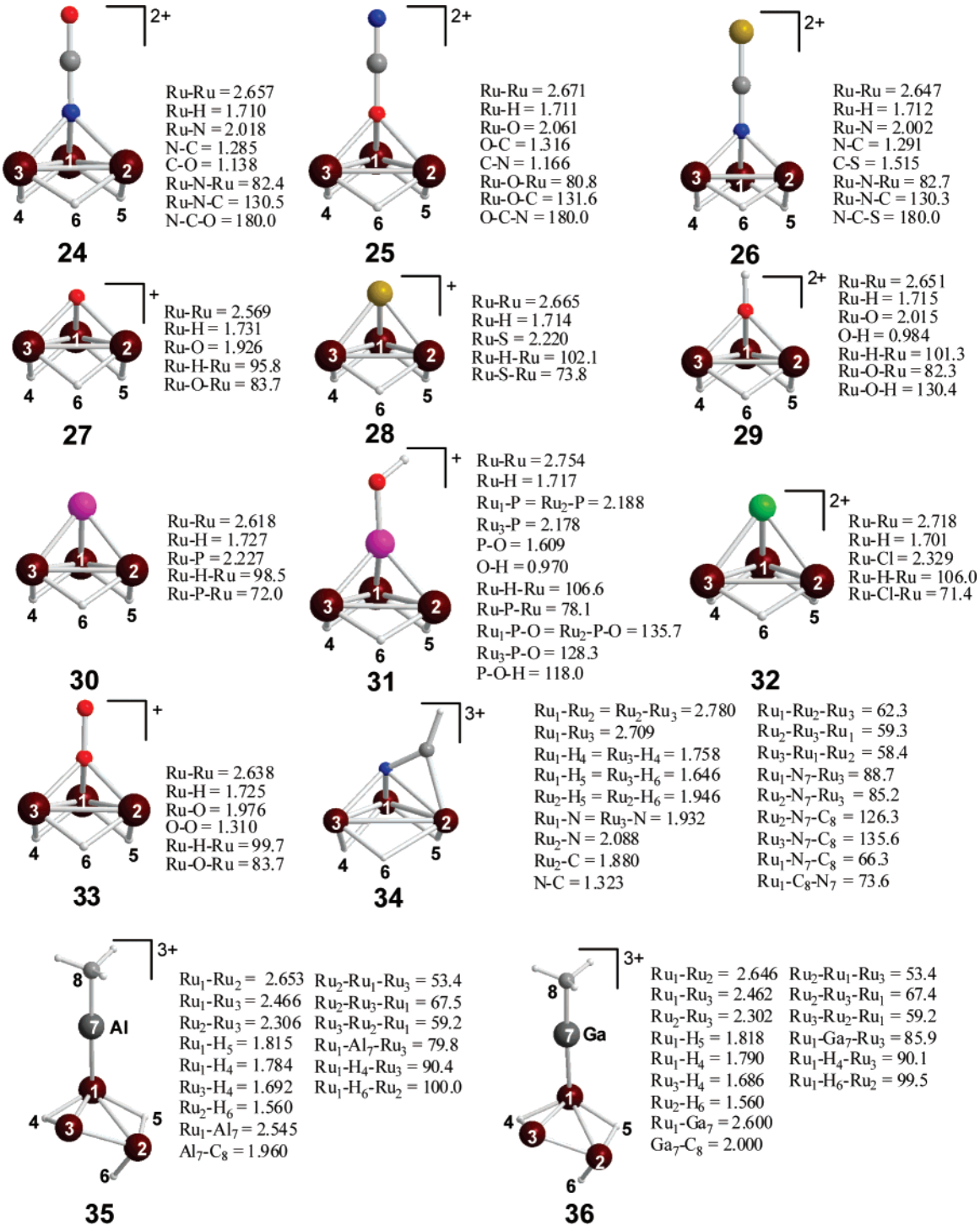

Figure 5. Equilibrium geometries (bond lengths in Å, angles in degrees) of [*cyclo*-$Ru_3(\mu\text{-H})_3(\mu_3\text{-Nuc})]^q$ (Nuc = NCO^-, **24**, OCN^-, **25**, NCS^-, **26**, O^{2-}, **27**, S^{2-}, **28**, OH^-, **29**, P^{3-}, **30**, POH^{2-}, **31**, Cl^-, **32**, O_2^{2-}, **33**, NCH, **34**, AlMe, **35**, GaMe, **36**; q = 0, +1, +2, +3) clusters computed at the B3P86/lanl2dz-(Ru)∪6-31++G**(E) (E = nonmetal element) level.

μ_3-C, μ_3-CH, and μ_3-CMe ligands introduced into the Ru_3 triangle, as is expected, enlarge the Ru_3 equilateral triangle with respect to the Ru_3 equilateral triangle of the parent [*cyclo*-$Ru_3(\mu\text{-H})_3]^{3+}$ molecule; the Ru−Ru bonds become longer by 0.08, 0.136, and 0.131 Å for **18**, **19**, and **20**, respectively. The same also holds true for clusters **21**, **22**, and **23**, which involve the triply bridging N^{3-}, NH^{2-}, and N_3^- ligands; the Ru−Ru bonds become longer by 0.085, 0.155, and 0.211 Å, respectively. Clusters **21**, **22**, and **23** have C_{3v} symmetry with the imido and azido ligands being perpendicularly coordinated on the Ru_3 triangle along the C_3 axis. Cluster **22** comprises the core structure of the "actual" [$(\eta^5\text{-}C_5Me_5)_3Ru_3(\mu\text{-H})_3(\mu_3\text{-NH})$] cluster obtained upon reacting the pentahydrido [$(\eta^5\text{-}C_5Me_5)_3Ru_3(\mu\text{-H})_3(\mu_3\text{-H})_2$] cluster with ammonia or hydrazine.[1i,n,o]

Clusters **24**, **25**, and **26**, belonging to C_{3v} point group, involve the triply bridging isocyanate, cyanate, and isothiocyanate ligands, all being perpendicularly coordinated on the Ru_3 triangle along the C_3 axis. The [*cyclo*-$Ru_3(\mu\text{-H})_3(\mu_3\text{-NCO})]^{2+}$ cluster is

predicted to be more stable than the [*cyclo*-$Ru_3(\mu\text{-H})_3(\mu_3\text{-OCN})]^{2+}$ isomer by 69.1 kcal/mol. In clusters **24**, **25**, and **26**, the Ru−Ru bond is elongated by 0.208, 0.222, and 0.198 Å, respectively. The greater elongation of the Ru−Ru bonds (amounted to 0.269 Å) occurs in cluster **32** with the triply bridging chloride ligand. Cluster **32** (C_{3v} symmetry) involves also the shorter symmetrical Ru−H−Ru hydrido bridge (Ru−H bond distance of 1.701 Å), which is much shorter than the Ru−H bond distance in the parent [*cyclo*-$Ru_3(\mu\text{-H})_3]^{3+}$ species by 0.091 Å. Cluster **32** comprises the core structure of the "actual" $[Ru_3(\eta^6\text{-}C_6H_2Me\text{-}1,2,4,6)_3(\mu\text{-H})_3(\mu_3\text{-Cl})]^{2+}$ triruthenium cluster, being accessible from the durene derivative $[Ru_2(\eta^6\text{-}C_6H_2Me\text{-}1,2,4,6)_2Cl_4)]$ by high-pressure hydrogenation (60 atm, 55 °C) in water.

Clusters **27**, **28**, and **29**, with C_{3v} symmetry, involve the triply bridging oxide, sulfide, and hydroxide ligands. Cluster **27** comprises the core structure of the "actual" $[Ru_3(\eta^6\text{-}C_6H_6)_3(\mu\text{-H})_3(\mu_3\text{-O})]^+$ and $[Ru_3(\eta^6\text{-}C_6H_6)(\eta^6\text{-}C_6Me_6)_2(\mu\text{-H})_3(\mu_3\text{-O})]^+$ triruthenium clusters. The former was obtained by low-pressure hydrogenation of the hydrolysis of $[Ru_2(\eta^6\text{-}C_6H_6)_2Cl_4)]$ in water (60 atm, 55 °C) in the presence of $NaClO_4$,[2a] whereas the later was synthesized by reacting $[Ru(\eta^6\text{-}C_6Me_6)(H_2O)_3]^{2+}$ with $[Ru_2(\eta^6\text{-}C_6Me_6)_2(\mu_2\text{-H})_3)]^+$ in aqueous solution.[2b] The $[Ru_3(\eta^6\text{-}C_6H_6)_3(\mu\text{-H})_3(\mu_3\text{-O})]^+$ cluster upon protonation affords the hydroxo-capped cluster $[Ru_3(\eta^6\text{-}C_6H_6)_3(\mu\text{-H})_3(\mu_3\text{-OH})]^+$.[2b] The chiral tetrahedral Ru_3O framework exists also in many other triruthenium clusters, such as the $[Ru_3(\eta^6\text{-}C_6H_6)(\eta^6\text{-}C_6Me_6)(\eta^6\text{-p-Pr}^iMeC_6H_4)(\mu\text{-H})_3(\mu_3\text{-O})]^+$ and $[Ru_3(\eta^6\text{-1-penylethanol})(\eta^6\text{-}C_6Me_6)(\eta^6\text{-p-Pr}^iMeC_6H_4)(\mu\text{-H})_3(\mu_3\text{-O})]^+$,[2i] and the $[Ru_3(\eta^6\text{-}endo\text{-Indanol})(\eta^6\text{-}C_6Me_6)_2(\mu_3\text{-O})]^+$ and $[Ru_3(\eta^6\text{-}exo\text{-Indanol})(\eta^6\text{-}C_6Me_6)_2(\mu_3\text{-O})]^+$ isomers.[1j] The oxo-capped clusters catalyze the hydrogenation of aromatic compounds in aqueous solution under biphasic conditions.[1h,2b,h] The sulfido-capped triruthenium core structure was found in the "actual" $[(\eta^5\text{-}C_5Me_5)_3Ru_3(\mu\text{-H})_3(\mu_3\text{-S})(\mu_3\text{-}CCH_2C_6H_5)]$ cluster resulted upon cleavage of carbon−sulfur bonds of benzothiophene and dibenzothiophene mediated by the pentahydrido $[(\eta^5\text{-}C_5Me_5)_3Ru_3(\mu\text{-H})_3(\mu_3\text{-H})_2]$ triruthenium cluster.[1b] Moreover, the triply bridging sulfide ligand was introduced into the Ru_3 core by the reaction of the $[(\eta^5\text{-}C_5Me_5)_3Ru_3(\mu\text{-H})_3(\mu_3\text{-H})_2]$ cluster with thiophenol.[1f] The sulfido-capped triruthenium core was also found in the dendridic cluster $[Ru_9S_8(cymene)_6]^{2+}$ obtained by condensation of $[Ru_3S_2(cymene)_3]^{2+}$ with sulfide. The Ru−O bond distance of 1.926 Å in the model cluster **27** is very close to the average Ru−O bond distance of 1.973 Å in the "actual" $[Ru_3(\eta^6\text{-}C_6H_2Me\text{-}1,2,4,6)_3(\mu\text{-H})_3(\mu_3\text{-O})]^{2+}$ triruthenium cluster.[2a] Similarly, the Ru−S bond distance of 2.220 Å in the model cluster **28** is very close to the average Ru−S bond distances of 2.286 and 2.276 Å in the "actual" $[(\eta^5\text{-}C_5Me_5)_3Ru_3(\mu\text{-H})_3(\mu_3\text{-S})(\mu_3\text{-}CCH_2C_6H_5)]$ and $[Ru_9S_8(cymene)_6]^{2+}$ clusters.[28] The slight shortening of the Ru−O and Ru−S bond distances in the model clusters could be explained on the grounds of the stronger interactions between the triply bridging oxide and sulfide ligands and the coordinatively unsaturated Ru(II) metal centers of the Ru_3 ring. In clusters **27**, **28**, and **29**, the Ru−Ru bonds are elongated by 0.120, 0.216, and 0.202 Å, respectively with respect to the Ru−Ru bonds of the parent [*cyclo*-$Ru_3(\mu\text{-H})_3]^{3+}$ cluster.

Clusters **30** and **31**, involving the triply bridging μ_3-P and μ_3-POH ligands, respectively, resemble the core structure of the "actual" $[Ru_3(CO)_9(\mu\text{-H})_2(\mu_3\text{-PPh})]$ triruthenium cluster.[4e] The average Ru−P bond distance in the "actual" cluster is 2.297 Å, whereas those in clusters **30** and **31** are 2.227 and 2.185 Å, respectively. The elongation of the Ru−Ru bonds in clusters **30** and **31** amounts to 0.169 and 0.305 Å, respectively.

The peroxo-$[O-O]^{2-}$ moiety was predicted to be coordinated with the Ru(II) atoms of the Ru_3 ring in a μ_3- end-on coordination mode with a perpendicular orientation with respect to the Ru_3 plane; thereby, cluster **33** exhibits C_{3v} symmetry. The μ_3-OO coordination to the Ru_3 ring elongates the Ru−Ru bonds by 0.189 Å.

Of particular interest is the coordination of HCN to the electron deficient Ru_3 ring. It is coordinated perpendicularly to one of the Ru−Ru bonds of the Ru_3 triangle in a $\mu_3\text{-}\eta^1(\perp)$-NCH coordination mode. This coordination mode differs from the coordination mode of nitriles, RCN, to the electron-rich Ru_3 ring, which corresponds also to a perpendicular to one of the Ru−Ru bonds coordination, but in a $\mu_3\text{-}\eta^2$: $\eta^2(\perp)$-RCN coordination mode.[1m] The HCN ligand in the model cluster **34** is triply bridging through the N donor atom, whereas in the "actual" nitrile clusters, the RCN ligands are triply bridging through the C donor atom. However, the average Ru−N bond distance of 1.971 Å is comparable to that of the "actual" $[(\eta^5\text{-}C_5Me_5)_3Ru_3(\mu_3\text{-}\eta^2\text{:}\eta^2(\perp)\text{-RCN})(\mu\text{-H})_3(\mu_3\text{-H})]^+$ (2.026 Å) and $[(\eta^5\text{-}C_5Me_5)_3Ru_3(\mu_3\text{-}\eta^2\text{:}\eta^2(\perp)\text{-RCNH})(\mu\text{-H})_3(\mu_3\text{-H})]^+$ (2.038 Å).[1m]

We also calculated the equilibrium geometries of clusters **35** and **36**, which involve ligands containing a metal atom, for example, AlMe and GaMe, respectively. Novel trinuclear ruthenium polyhydride complexes with a triply bridging metal alkyl ligand formulated as $[(\eta^5\text{-}C_5Me_5)_3Ru_3(\mu_3\text{-M})(\mu\text{-H})_3]$ (M = AlEt and GaMe) have been recently synthesized and structurally characterized, and their influences on the reactivity of the clusters has been evaluated by means of cyclic voltametry.[1g] In contrast to the "actual" $[(\eta^5\text{-}C_5Me_5)_3Ru_3(\mu_3\text{-M})(\mu\text{-H})_3]$ (M = AlEt and GaMe) clusters in the model clusters **35** and **36**, the metal alkyl ligands are coordinated with only one Ru(II) metal center of the Ru_3 ring. The Ru−Ga bond distance of 2.646 Å in the model cluster **36** is much longer than the average Ru−Ga bond distance of 2.47 Å in the "actual" $[(\eta^5\text{-}C_5Me_5)_3Ru_3(\mu_3\text{-GaMe})(\mu\text{-H})_3]$ clusters.

Finally, we calculated the equilibrium geometries of two more model clusters involving a face-capping benzene ligand, **37**, and a face-capping $\mu_3\text{-}\eta^3\text{-}C_3$ ring, **38** (Figure 6). The novel facial benzene complex $[(\eta^5\text{-}C_5Me_5)_3Ru_3(\mu\text{-H})_3(\mu_3\text{-}\eta^2\text{:}\eta^2\text{:}\eta^2\text{-}C_6H_6)]$ has been well characterized,[29] whereas the mechanistic aspects of formation of the face-capping $\mu_3\text{-}C_3$ ring on the triruthenium plane of trinuclear cluster of ruthenium as a consequence of bimetallic reductive C−C coupling has been reported recently. The $\mu_3\text{-}\eta^3\text{-}C_3$ ring was structurally characterized for the monocationic complex $[(\eta^5\text{-}C_5Me_5)_3Ru_3(\mu_3\text{-CH})(\mu_3\text{-}\eta^3\text{-}C_3H_2Me)]^+$. In spite of the unsaturation of the model [*cyclo*-$Ru_3(\mu\text{-H})_3]^{3+}$ cluster, the structural cores of the model clusters **37** and **38** closely resemble those of the "actual" $[(\eta^5\text{-}C_5Me_5)_3Ru_3(\mu\text{-H})_3(\mu_3\text{-}\eta^2\text{:}\eta^2\text{:}\eta^2\text{-}C_6H_6)]$ and $[(\eta^5\text{-}C_5Me_5)_3Ru_3(\mu_3\text{-CH})(\mu_3\text{-}\eta^3\text{-}C_3H_2Me)]^+$ complexes. Thus, the $\mu_3\text{-}\eta^2\text{:}\eta^2\text{:}\eta^2$-bonded benzene molecule adopts the staggered conformation with respect to the Ru_3

(28) Kuhlman, M. L.; Rauchfuss, T. B. *Organometallics* **2004**, *23*, 5085.

(29) Inagaki, A.; Takaya, Y.; Takemori, T.; Suzuki, H. *J. Am. Chem. Soc.* **1997**, *119*, 625.

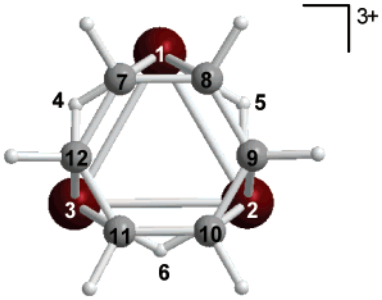

37

Ru_1-Ru_2 = Ru_1-Ru_3 = 2.827
Ru_2-Ru_3 = 2.820
Ru-H = 1.670
Ru-C = 2.177
C_7-C_8 = C_9-C_{10} = C_{11}-C_{12} = 1.417
C_8-C_9 = C_{10}-C_{11} = C_7-C_{12} = 1.467
Ru-H-Ru = 115.5
C-Ru-C = 38.0
Ru-C-C = 71.0

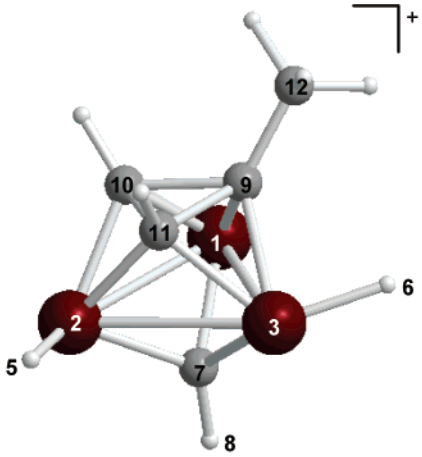

38

Ru_1-Ru_2 = 2.838
Ru_1-Ru_3 = 2.835
Ru_2-Ru_3 = 2.843
Ru-H = 1.589
Ru-C_7 = 1.972
Ru_1-C_9 = Ru_2-C_{10} = 2.038
Ru_1-C_{10} = Ru_2-C_{11} = Ru_3-C_9 = 1.992
Ru_3-C_{11} = 2.031
C_9-C_{10} = 1.614
C_9-C_{11} = 1.624
C_{10}-C_{11} = 1.570
C_9-C_{12} = 1.494

Ru-Ru-Ru = 60.0
Ru_1-Ru_3-C_9 = 46.0
Ru_1-C_9-Ru_3 = 89.4
C_{10}-C_{11}-C_9 = 58.0
C_9-C_{10}-C_{11} = 61.3
C_{11}-C_9-C_{12} = 121.3
Ru_1-C_7-Ru_3 = 92.0

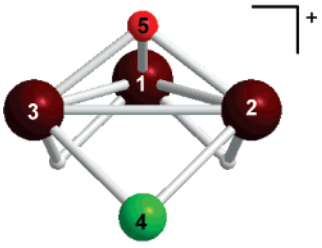

40

Ru_1-Ru_2 = Ru_1-Ru_3 = 2.595
Ru_2-Ru_3 = 3.076
Ru_2-Cl_4 = Ru_3-Cl_4 = 2.350
Ru_2-O_5 = Ru_3-O_5 = 1.962
Ru_1-O_5 = 1.919
Ru_1-H = 1.745
Ru_2-H = Ru_3-H = 1.724
Ru_2-Ru_1-Ru_3 = 72.7
Ru_2-Cl_4-Ru_3 = 81.8
Ru_2-O_5-Ru_3 = 103.2
Ru_1-O_5-Ru_2 = Ru_1-O_5-Ru_3 = 83.9
Ru_1-H-Ru_2 = Ru_1-H-Ru_3 = 96.8

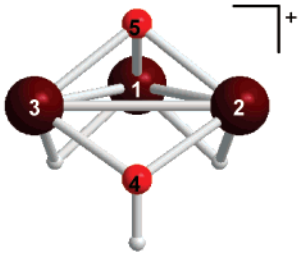

41

Ru_1-Ru_2 = Ru_1-Ru_3 = 2.602
Ru_2-Ru_3 = 2.985
Ru_2-O_4 = Ru_3-O_4 = 2.016
Ru_2-O_5 = Ru_3-O_5 = 1.960
Ru_1-O_5 = 1.912
Ru_1-H = 1.741
Ru_2-H = Ru_3-H = 1.735
Ru_2-Ru_1-Ru_3 = 70.0
Ru_2-O_4-Ru_3 = 95.5
Ru_2-O_5-Ru_3 = 99.2
Ru_1-O_5-Ru_2 = Ru_1-O_5-Ru_3 = 84.5
Ru_1-H-Ru_2 = Ru_1-H-Ru_3 = 97.0

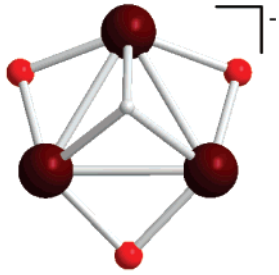

42

Ru-Ru = 2.582
Ru-H = 1.896
Ru-O = 1.885
Ru-H-Ru = 85.8
Ru-O-Ru = 86.4

Figure 6. Equilibrium geometries (bond lengths in Å, angles in degrees) of [*cyclo*-$Ru_3(\mu\text{-H})_3(\mu_3\text{-}\eta^2\text{:}\eta^2\text{:}\eta^2\text{-}C_6H_6)]^{3+}$, **37**, and [*cyclo*-$Ru_3(\mu\text{-H})(\mu_3\text{-CH})(\mu_3\text{-}\eta^3\text{-}C_3H_2Me]^{+}$, **38**, clusters computed at the B3P86/lanl2dz(Ru)∪6-31++G**(E) (E = nonmetal element) level.

ring as in the case of "actual" complex exhibiting Ru−C bond distances of 2.177 Å (the average Ru−C bond distance in the "actual" complex is 2.197 Å).[29] The C−C bonds of the coordinated benzene molecule are not equivalent; three of them acquire a bond lengths of 1.417 Å and the other alternate three ones aquire bond lengths of 1.467 Å. Similarly, the μ_3-η^3-C_3 ring in cluster **38** adopts also the staggered conformation with respect to the Ru_3 ring, as in the case of "actual" complex with average Ru−C bond distance of 2.016 Å (the average Ru−C bond distance in the "actual" complex is 2.065 Å).[30b] The Ru−C bond distance in the triply bridging carbyne ligand, CH, of **38** is 1.972 Å, whereas the average Ru−C bond distance in the "actual" complex is 2.009 Å.

The most striking structural feature of cluster **38** is the very long nonequivalent C−C bonds in the coordinated C_3 ring. The 3-membered carbon atom ring forms a nearly isosceles triangle

Table 4. Bond Dissociation Energies, *DE*s (in kcal/mol), and Interaction Energies, *IE*s (in kcal/mol), between the [*cyclo*-$Ru_3(\mu_2\text{-H})_3]^{3+}$ and Nuc Fragments of the [*cyclo*-$Ru_3(\mu\text{-H})_3(\mu_3\text{-Nuc})]^q$ Clusters Computed at the B3P86/lanl2dz(Ru)∪6-31++G**(E) (*E* = Nonmetal Element) Level

cluster	*DE*	*IE*	cluster	*DE*	*IE*
$[Ru_3(\mu_2\text{-H})_3(\mu_3\text{-BH})]^{3+}$, **15**	180.8	−199.8	$[Ru_3(\mu_2\text{-H})_3(\mu_3\text{-O})]^{+}$, **27**	1038.1	−1229.7
$[Ru_3(\mu_2\text{-H})_3(\mu_3\text{-BCN})]^{3+}$, **16**	177.5	−199.9	$[Ru_3(\mu_2\text{-H})_3(\mu_3\text{-S})]^{+}$, **28**	949.9	−1044.9
$[Ru_3(\mu_2\text{-H})_3(\mu_3\text{-BOMe})]^{3+}$, **17**	187.6	−212.4	$[Ru_3(\mu_2\text{-H})_3(\mu_3\text{-OH})]^{2+}$, **29**	533.5	−611.3
$[Ru_3(\mu_2\text{-H})_3(\mu_3\text{-C})]^{-}$, **18**	1808.0	−2607.5	$[Ru_3(\mu_2\text{-H})_3(\mu_3\text{-P})]$, **30**	1333.4	−1557.2
$[Ru_3(\mu_2\text{-H})_3(\mu_3\text{-CH})]$, **19**	1408.7	−1849.8	$[Ru_3(\mu_2\text{-H})_3(\mu_3\text{-POH})]^{+}$, **31**	981.3	−1113.0
$[Ru_3(\mu_2\text{-H})_3(\mu_3\text{-CMe})]$, **20**	1356.2	−1760.6	$[Ru_3(\mu_2\text{-H})_3(\mu_3\text{-Cl})]^{2+}$, **32**	471.0	−514.5
$[Ru_3(\mu_2\text{-H})_3(\mu_3\text{-N})]$, **21**	1514.3	−1941.1	$[Ru_3(\mu_2\text{-H})_3(\mu_3\text{-OO})]^{+}$, **33**	941.7	−1096.4
$[Ru_3(\mu_2\text{-H})_3(\mu_3\text{-NH})]^{3+}$, **22**	216.1	−247.8	$[Ru_3(\mu_2\text{-H})_3(\mu_3\text{-}\eta^2\text{-NCH})]^{3+}$, **34**	110.5	−159.9
$[Ru_3(\mu_2\text{-H})_3(\mu_3\text{-N}_3)]^{2+}$, **23**	505.6	−569.3	$[Ru_3(\mu_2\text{-H})_3(\mu\text{-AlMe})]^{3+}$, **35**	183.9	−200.4
$[Ru_3(\mu_2\text{-H})_3(\mu_3\text{-NCO})]^{2+}$, **24**	495.8	−561.2	$[Ru_3(\mu_2\text{-H})_3(\mu\text{-GaMe})]^{3+}$, **36**	184.8	−195.8
$[Ru_3(\mu_2\text{-H})_3(\mu_3\text{-OCN})]^{2+}$, **25**	426.8	−479.8	$[Ru_3(\mu\text{-H})_3(\mu_3\text{-}\eta^2\text{:}\eta^2\text{:}\eta^2\text{-}C_6H_6)]^{3+}$, **37**	208.5	−280.9
$[Ru_3(\mu_2\text{-H})_3(\mu_3\text{-NCS})]^{2+}$, **26**	496.2	−558.9	$[Ru_3(\mu\text{-H})_3(\mu_3\text{-CH})(\mu_3\text{-}\eta^3\text{-}C_3H_2Me]^{+}$, **38**	268.5	−288.7

Table 5. Selected Electronic Parameters of the [*cyclo*-$Ru_3(\mu\text{-H})_3(\mu_3\text{-Nuc})]^q$ Clusters Computed at the B3P86/lanl2dz(Ru)∪6-31++G**(E) (*E* = Nonmetal Element) Level

cluster	ϵ_{HOMO}	ϵ_{LUMO}	*q*(Nuc)[a]	net charge donation[b] $CT_{2\to1}$ - $CT_{1\to2}$	Mayer bond orders[c]
$[Ru_3(\mu_2\text{-H})_3(\mu_3\text{-BH})]^{3+}$, **15**	−24.001	−21.871	0.494	0.230	3.540
$[Ru_3(\mu_2\text{-H})_3(\mu_3\text{-BCN})]^{3+}$, **16**	−23.667	−21.650	0.354	0.359	3.564
$[Ru_3(\mu_2\text{-H})_3(\mu_3\text{-BOMe})]^{3+}$, **17**	−22.404	−20.323	0.588	0.593	2.672
$[Ru_3(\mu_2\text{-H})_3(\mu_3\text{-C})]^{-}$, **18**	−0.128	1.458	−0.356	3.765	3.340
$[Ru_3(\mu_2\text{-H})_3(\mu_3\text{-CH})]$, **19**	−4.939	−2.755	−0.170	2.731	2.922
$[Ru_3(\mu_2\text{-H})_3(\mu_3\text{-CMe})]$, **20**	−4.773	−2.601	−0.135	2.739	2.936
$[Ru_3(\mu_2\text{-H})_3(\mu_3\text{-N})]$, **21**	−5.349	−3.059	−0.489	2.410	2.882
$[Ru_3(\mu_2\text{-H})_3(\mu_3\text{-NH})]^{3+}$, **22**	−23.936	−22.740	−0.110	0.371	2.236
$[Ru_3(\mu_2\text{-H})_3(\mu_3\text{-N}_3)]^{2+}$, **23**	−16.557	−13.906	0.070	0.811	1.804
$[Ru_3(\mu_2\text{-H})_3(\mu_3\text{-NCO})]^{2+}$, **24**	−16.754	−14.058	0.009	0.853	1.672
$[Ru_3(\mu_2\text{-H})_3(\mu_3\text{-OCN})]^{2+}$, **25**	−17.557	−14.818	−0.234	0.765	1.386
$[Ru_3(\mu_2\text{-H})_3(\mu_3\text{-NCS})]^{2+}$, **26**	−15.992	−13.474	0.146	0.966	1.862
$[Ru_3(\mu_2\text{-H})_3(\mu_3\text{-O})]^{+}$, **27**	−11.402	−8.861	−0.528	1.389	2.114
$[Ru_3(\mu_2\text{-H})_3(\mu_3\text{-S})]^{+}$, **28**	−11.363	−8.831	0.180	2.283	2.948
$[Ru_3(\mu_2\text{-H})_3(\mu_3\text{-OH})]^{2+}$, **29**	−17.200	−14.486	−0.188	0.766	1.346
$[Ru_3(\mu_2\text{-H})_3(\mu_3\text{-P})]$, **30**	−5.470	−3.163	0.173	3.264	3.302
$[Ru_3(\mu_2\text{-H})_3(\mu_3\text{-POH})]^{+}$, **31**	−10.818	−8.470	0.629	2.561	3.314
$[Ru_3(\mu_2\text{-H})_3(\mu_3\text{-Cl})]^{2+}$, **32**	−17.598	−14.884	0.120	1.296	1.966
$[Ru_3(\mu_2\text{-H})_3(\mu_3\text{-OO})]^{+}$, **33**	−11.599	−9.111	−0.483	1.414	2.194
$[Ru_3(\mu_2\text{-H})_3(\mu_3\text{-}\eta^2\text{-NCH})]^{3+}$, **34**	−23.087	−21.180	0.233	0.064	3.096
$[Ru_3(\mu_2\text{-H})_3(\mu\text{-AlMe})]^{3+}$, **35**	−21.570	−19.657	1.273	1.381	1.196
$[Ru_3(\mu_2\text{-H})_3(\mu\text{-GaMe})]^{3+}$, **36**	−21.415	−19.494	1.266	1.197	0.956
$[Ru_3(\mu\text{-H})_3(\mu_3\text{-}\eta^2\text{:}\eta^2\text{:}\eta^2\text{-}C_6H_6)]^{3+}$, **37**	−21.244	−18.741	0.823	1.149	4.004
$[Ru_3(\mu\text{-H})_3(\mu_3\text{-CH})(\mu_3\text{-}\eta^3\text{-}C_3H_2Me]^{+}$, **38**	−11.150	−7.993	0.138	1.085	4.912

[a] Natural atomic charges. [b] Mulliken net atomic charges. [c] Mayer bond orders refer to the sum of the three Ru−Nuc bonds.

with sides of 1.614, 1.624, and 1.570 Å. Notably, these C−C bonds are significantly longer than the normal C−C single bonds with a C−C bond length of 1.537 Å.

Stability and Bonding Properties of the [*cyclo*-$Ru_3(\mu\text{-H})_3(\mu_3\text{-Nuc})]^q$ (Nuc = BH, BCN, BOMe, C^{4-}, CH^{3-}, CMe^{3-}, N^{3-}, NH, N_3^-, OCN^-, SCN^-, O^{2-}, S^{2-}, OH^-, P^{3-}, POH^{2-}, Cl^-, O_2^{2-}, NCH, AlMe, GaMe; $q = -1, 0, +1, +2$) Clusters. The stability of the [*cyclo*-$Ru_3(\mu\text{-H})_3(\mu_3\text{-Nuc})]^q$ molecules are investigated using the following fragmentation scheme:

$$[cyclo\text{-}Ru_3(\mu\text{-H})_3(\mu_3\text{-Nuc})]^q \rightarrow [cyclo\text{-}Ru_3(\mu\text{-H})_3]^{3+} + Nuc^{q'}$$

The calculated dissociation energies (*DE*s) are compiled in Table 4 along with the interaction energies (without BSSE corrections) between the [*cyclo*-$Ru_3(\mu_2\text{-H})_3]^{3+}$ and Nuc fragments computed by charge decomposition analysis as implemented in the AOMix program.[15,16]

It can be seen that the calculated dissociation energies (*DE*s) are in all cases lower than the absolute values of the interaction energies (without BSSE corrections) between the [*cyclo*-$Ru_3(\mu_2\text{-H})_3]^{3+}$ and Nuc fragments. This is an expected result, for the *DE*s correspond to the dissociation of the [*cyclo*-$Ru_3(\mu\text{-H})_3(\mu_3\text{-Nuc})]^q$ molecules to the [*cyclo*-$Ru_3(\mu\text{-H})_3]^{3+}$ and $Nuc^{q'}$ fragments in their relaxed ground state geometries. On the other hand, the interaction energies correspond to the association of the [*cyclo*-$Ru_3(\mu\text{-H})_3]^{3+}$ and $Nuc^{q'}$ fragments keeping the geometries they have in the [*cyclo*-$Ru_3(\mu\text{-H})_3(\mu_3\text{-Nuc})]^q$ molecules. According to both the estimated *DE*s and interaction energies (*IE*s), the nucleophiles Nuc are strongly bonded to the Ru_3 ring of the [*cyclo*-$Ru_3(\mu_2\text{-H})_3]^{3+}$ species. For the neutral nucleophiles (BH, BCN, BOMe, NH, NCH, AlMe, and GaMe) the *DE*s range from 110.5 to 216.1 kcal/mol, whereas the *IE*s range from −159.9 to −247.8 kcal/mol. In both cases, the stability of the respective clusters follows the trend: NH > BOMe > BH ≈ AlMe ≈ GaMe ≈ BCN. For the anionic nucleophiles, the *DE*s are much higher than those of the neutral ones, because of the high-energy demand to separate the

(30) (a) Takao, T.; Inagaki, A.; Murotani, E.; Imamura, T.; Suzuki, H. *Organometallics* **2003**, *22*, 1361. (b) Takao, T.; Moriya, M.; Suzuki, H. *Organometallics* **2007**, *26*, 1349. (c) Moriya, M.; Takao, T.; Suzuki, H. *Organometallics* **2007**, *26*, 1650.

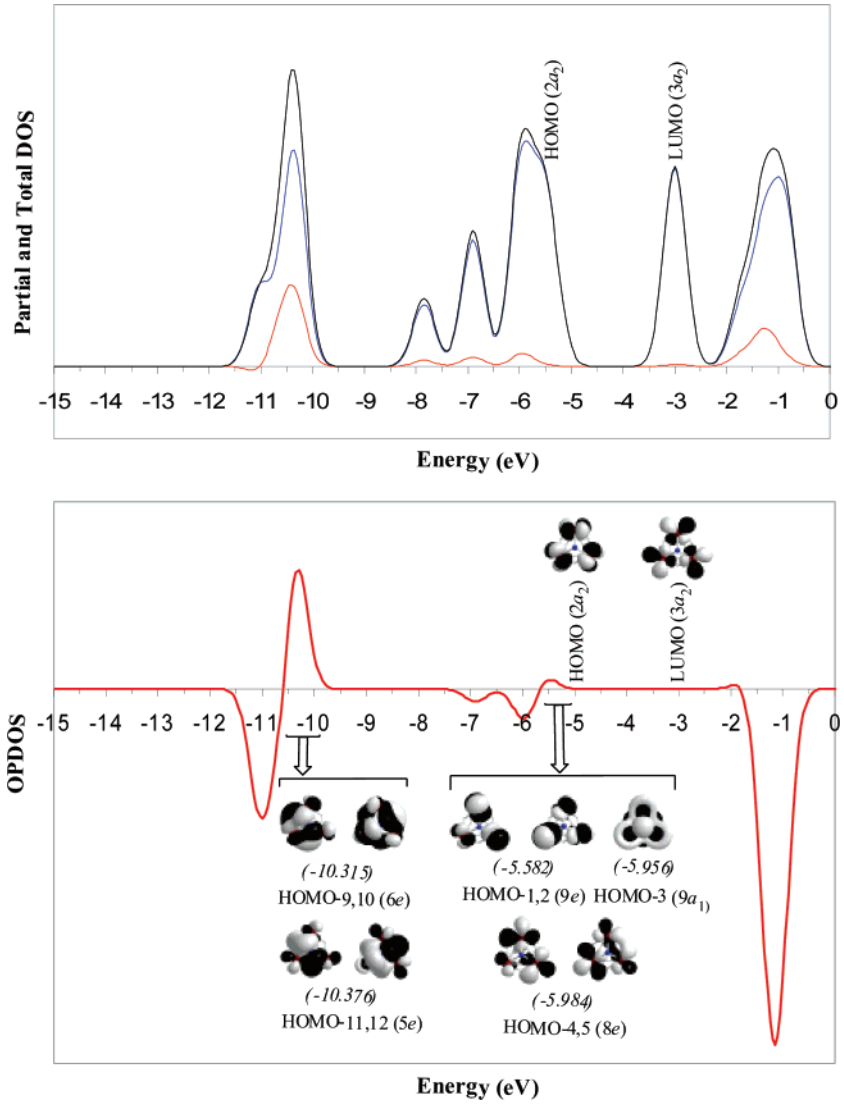

Figure 7. Density-of-states (DOS) and overlap population DOS (OPDOS) plots along with the shapes of the most relevant valence molecular orbitals of a representative cluster, [*cyclo*-$Ru_3(\mu\text{-H})_3(\mu_3\text{-N})]^+(C_{3v})$, **21**, computed at the B3P86/lanl2dz(Ru)∪6-31++G**(E) (*E* = nonmetal element) level.

oppositely charged fragments. The same also holds true for the *IE*s being much higher for the anionic than the neutral nucleophiles, because of the strong electrostatic (Coulomb) interactions between the oppositely charged species. Notably, the higher the negative charge of the nucleophile, the higher the *DE*s and *IE*s. For the monoanionic nucleophiles (N_3^-, NCO^-, OCN^-, NCS^-, OH^-, Cl^-), the *DE*s range from 471.0 to 533.5 kcal/mol, whereas the *IE*s range from −514.5 to −611.3 kcal/mol and follow the trend: $OH^- > N_3^- > NCS^- \approx NCO^- > OCN^- > Cl^-$. For the dianionic nucleophiles (O^{2-}, S^{2-}, POH^{2-}, and OO^{2-}) with *DE*s and *IE*s in the range of 941.7 to 1038.1 kcal/mol and −1096.4 to −1229.7 kcal/mol, respectively, the trend followed is: $O^{2-} > POH^{2-} > S^{2-} > OO^{2-}$. For the trianionic nucleophiles (CH^{3-}, CMe^{3-}, N^{3-}, and P^{3-}) with *DE*s and *IE*s in the range of 1333.4 to 1514.3 kcal/mol and −1557.2 to −1941.1 kcal/mol, the trend followed is: $N^{3-} > CH^{3-} > CMe^{3-} > P^{3-}$. Finally, the tetraanionic C^{4-} nucleophile exhibits the highest *DE* (1808.0 kcal/mol) and lowest *IE* (−2607.5 kcal/mol).

Let us now analyze the μ_3-Nuc bonding mode in the [*cyclo*-$Ru_3(\mu\text{-H})_3(\mu_3\text{-Nuc})]^q$ molecules. Selected electronic parameters of the [*cyclo*-$Ru_3(\mu\text{-H})_3(\mu_3\text{-Nuc})]^q$ clusters computed at the B3P86/lanl2dz(Ru)∪6-31++G**(E) (E = nonmetal element) level are given in Table 5.

Perusal of Table 5 reveals that there is a strong charge transfer from the Nuc to the Ru_3 ring. The net charge donation estimated by the CDA calculations amounts to 0.064−3.765 |e|. The lower charge transfer donation occurs in the μ_3-NCH cluster, and the highest one occurs in the μ_3-C cluster. The charge transfer donation to the Ru_3 ring has as a consequence of the dramatic lowering of the electron density on the μ_3-bridging unit. For example, in the [*cyclo*-$Ru_3(\mu\text{-H})_3(\mu_3\text{-O})]^+$, **27**, cluster, the triply bridging oxide donor atom acquires a negative natural atomic charge of −0.528 |e| because of the transfer of 1.472 |e| of natural charge to the Ru_3 ring. The net charge donation of 1.389 |e| is slightly different because the net charge donation corresponds to Mulliken net atomic charges.

For the tricationic species, the net charge donation follows the trend AlMe > GaMe > C_6H_6 > BOMe > NH > BCN > BH > NCH, whereas for the di- and monocationic clusters, the trends followed are $Cl^- > NCS^- > NCO^- > N_3^- > OCN^- \approx OH^-$ and $POH^{2-} > S^{2-} > O_2^{2-} > O^{2-}$, respectively. Finally, for the neutral clusters, the net charge donation follows the trend $P^{3-} > CMe^{3-} > CH^{3-} > N^{3-}$. The estimated Mayer bond orders

Scheme 3. Most Relevant Valence Molecular Orbitals of [*cyclo*-$Ru_3(\mu\text{-H})_3(\mu_3\text{-O})]^+(C_{3v})$, **27**

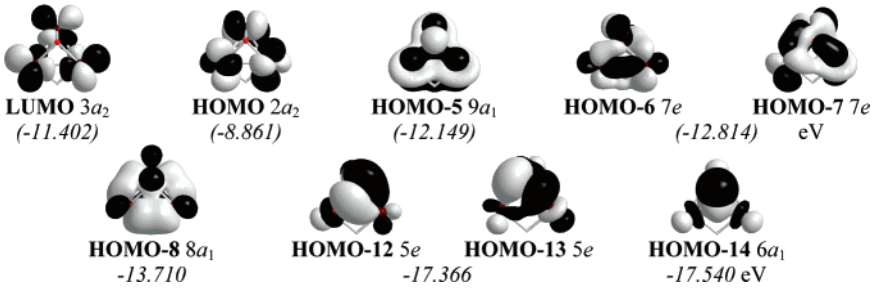

Scheme 4. Most Relevant Valence Molecular Orbitals of [*cyclo*-$Ru_3(\mu\text{-H})_3(\mu_3\text{-}\eta^2\text{:}\eta^2\text{:}\eta^2\text{-}C_6H_6)]^{3+}$, **37**

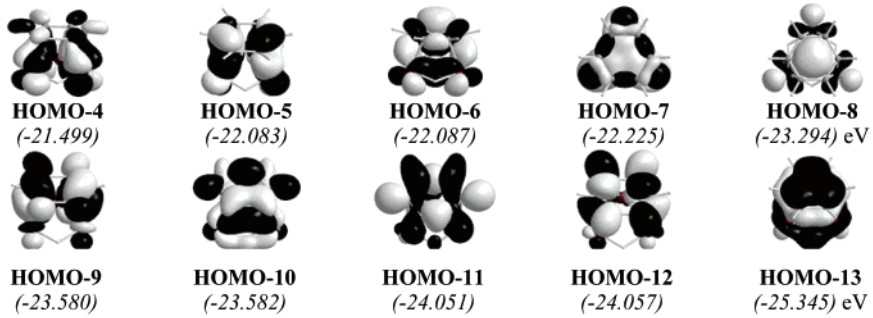

Scheme 5. Most Relevant Valence Molecular Orbitals of the [*cyclo*-$Ru_3(\mu\text{-H})(\mu_3\text{-CH})(\mu_3\text{-}\eta^3\text{-}C_3H_2Me)$] Cluster, **38**

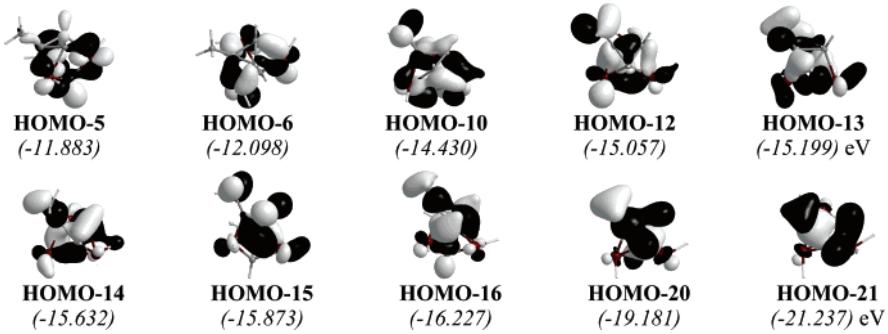

using CDA range from 0.956 in the CaMe cluster, **36**, to 4.912 in the η^3-C_3H_2Me cluster, **38**. The GaMe and AlMe nucleophiles, having Mayer bond orders around 1.0, are singly bonded to one of the Ru(II) metal atoms of the Ru_3 ring. Furthermore, from the Mayer bond order values one may conclude that most of the bridging nucleophiles (BH, BCN, BOMe, C^{4-}, CH^{3-}, CMe^{3-}, N^{3-}, S^{2-}, P^{3-}, POH^{2-}, NCH, C_6H_6, and η^3-C_3H_2Me) are strongly bonded to the Ru_3 ring (Mayer bond orders values around 3.0). The rest of the nucleophiles with Mayer bond orders values around 2.0 (NH, N_3^-, NCO^-, OCN^-, NCS^-, O^{2-}, OH^-, Cl^-, and O_2^{2-}) are less strongly bonded to the Ru_3 ring.

The composition of the $Ru_3(\mu_3\text{-Nuc})$ natural bonds of the [*cyclo*-$Ru_3(\mu\text{-H})_3(\mu_3\text{-Nuc})]^q$ clusters are compiled in Table S1 (Supporting Information). A thorough inspection of the Ru_3-$(\mu_3\text{-Nuc})$ natural bonds of the [*cyclo*-$Ru_3(\mu\text{-H})_3(\mu_3\text{-Nuc})]^q$ clusters indicates that they are constructed by in-phase interaction of Ru_3 group orbitals (involving various combinations of the 5d orbitals of the Ru atoms) with sp^x ($x = 1.92-3.95$) hybridized or with linear combination of the *n*p orbitals of the donor atom of the nucleophile. A clear picture of the bonding mechanism in the [*cyclo*-$Ru_3(\mu\text{-H})_3(\mu_3\text{-Nuc})]^q$ clusters is provided by the density-of-states (DOS) and overlap population density-of-states (OPDOS) plots along with the most relevant valence molecular orbitals of a representative cluster [*cyclo*-$Ru_3(\mu\text{-H})_3(\mu_3\text{-N})]^+(C_{3v})$, **21**, are shown in Figure 7. The DOS and OPDOS plots were generated using Gaussian functions with half-widths of 0.5 eV. These plots provide pictorial representation of molecular orbital (MO) compositions and their contributions to chemical bonding. Analogous plots are obtained for all [*cyclo*-$Ru_3(\mu\text{-H})_3(\mu_3\text{-Nuc})]^q$ clusters.

The OPDOS plot illustrates that both the lowest unoccupied (LUMO) and highest occupied molecular orbitals (HOMO) are nonbonding MOs localized on the triangular Ru_3 ring. The same holds true for the doubly degenerate HOMO-1,2 (9*e*) and HOMO-4,5 (8*e*), whereas the molecular orbitals that are relevant for the $Ru_3(\mu_3\text{-N})$ bonding are the doubly degenerate HOMO-9,10 (6*e*) and HOMO-11,12 (5*e*), with eigenvalues of -10.315 and -10.376 eV, respectively. These MOs are constructed from 2p orbitals of the triply bridged μ_3-N^{3-} interacting in-phase with MOs of appropriate symmetry localized on the Ru_3 ring. The respective orbitals of the analogous [*cyclo*-$Ru_3(\mu\text{-H})_3(\mu^3\text{-O})]^+$ (C_{3v}), **27**, are shown in Scheme 3.

Noteworthy is the bonding mechanism in the μ_3-η^2:η^2:η^2-C_6H_6 and μ_3-η^3-C_3H_2Me triply bridging Ru_3 ring. The benzene

molecule adopts a Kekule structure with each double bond coordinated to a Ru(II) atom of the Ru_3 ring in a η^2-fashion. The composition of the two Ru−C natural bonds, that is, Ru_1-C_7 and Ru_1-C_8 (Figure 6), formed upon interaction of the benzene double bond with the Ru(II) atom are given below:

$$\mathbf{Ru_1-C_7} = \mathbf{0.796}(0.198|s\rangle + 0.739|xy\rangle + 0.156|xz\rangle + 0.558|x^2-y^2\rangle - 0.270|z^2\rangle)_{\mathbf{Ru}} + \mathbf{0.605}(0.229|s\rangle - 0.957|x\rangle)_{\mathbf{C}}$$

$$\mathbf{Ru_1-C_8} = \mathbf{0.785}(-0.232|s\rangle + 0.486|xy\rangle + 0.488|xz\rangle - 0.256|yz\rangle - 0.620|x^2-y^2\rangle + 0.126|z^2\rangle)_{\mathbf{Ru}} + \mathbf{0.620}(-0.229|s\rangle + 0.957|x\rangle - 0.151|z\rangle)_{\mathbf{C}}$$

The pictures of the molecular orbitals that are relevant for the $Ru_3(\mu_3\text{-}\eta^2\text{:}\eta^2\text{:}\eta^2\text{-}C_6H_6)$ bonding in the [*cyclo*-$Ru_3(\mu\text{-H})_3(\mu_3\text{-}\eta^2\text{:}\eta^2\text{:}\eta^2\text{-}C_6H_6)]^{3+}$ cluster, **37**, are shown in Scheme 4.

It is clear that orbital interactions and not π-π stacking-like interactions are the driving forces for the strong association of the benzene ring with the antiaromatic Ru_3 ring. The same holds true for the mechanism of the bonding in the $[Ru_3(\mu\text{-H})(\mu_3\text{-CH})(\mu_3\text{-}\eta^3\text{-}C_3H_2Me]$ cluster, **38**. The η^3-C_3 ring is strongly associated with the Ru_3 ring primarily through the appropriate orbital interactions. The composition of the Ru−C natural bonds formed, that is, Ru_1-C_{10}, Ru_1-C_{11}, Ru_2-C_9, Ru_2-C_{10}, and Ru_3-C_9 (Figure 6), are given below:

$$\mathbf{Ru_1-C_{10}} = \mathbf{0.670}(0.454|xy\rangle - 0.572|xz\rangle - 0.430|yz\rangle + 0.257|x^2-y^2\rangle + 0.190|z^2\rangle)_{\mathbf{Ru}} + \mathbf{0.742}(0.426|s\rangle + 0.708|x\rangle - 0.185|y\rangle - 0.528|z\rangle)_{\mathbf{C}}$$

$$\mathbf{Ru_1-C_{11}} = \mathbf{0.608}(-0.596|s\rangle + 0.614|xy\rangle + 0.341|xz\rangle - 0.335|yz\rangle + 0.188|z^2\rangle)_{\mathbf{Ru}} + \mathbf{0.794}(-0.442|s\rangle - 0.604|x\rangle - 0.257|y\rangle + 0.607|z\rangle)_{\mathbf{C}}$$

$$\mathbf{Ru_2-C_9} = \mathbf{0.850}(0.327|xy\rangle + 0.707|xz\rangle - 0.541|yz\rangle + 0.272|x^2-y^2\rangle - 0.131|z^2\rangle)_{\mathbf{Ru}} + \mathbf{0.528}(-0.329|s\rangle + 0.117|x\rangle + 0.480|y\rangle + 0.574|z\rangle)_{\mathbf{C}}$$

$$\mathbf{Ru_2-C_{10}} = \mathbf{0.796}(0.487|xy\rangle - 0.552|xz\rangle - 0.606|x^2-y^2\rangle + 0.245|z^2\rangle)_{\mathbf{Ru}} + \mathbf{0.606}(-0.229|s\rangle + 0.957|x\rangle + 0.151|z\rangle)_{\mathbf{C}}$$

$$\mathbf{Ru_3-C_9} = \mathbf{0.839}(-0.284|s\rangle - 0.532|xy\rangle + 0.455|xz\rangle + 0.290|yz\rangle + 0.283|x^2-y^2\rangle + 0.514|z^2\rangle)_{\mathbf{Ru}} + \mathbf{0.545}(-0.325|s\rangle + 0.228|x\rangle - 0.370|y\rangle + 0.652|z\rangle)_{\mathbf{C}}$$

The pictures of the molecular orbitals that are relevant for the $Ru_3(\mu_3\text{-}\eta^3\text{-}C_3H_2Me)$ bonding in the $[Ru_3(\mu\text{-H})(\mu_3\text{-CH})(\mu_3\text{-}\eta^3\text{-}C_3H_2Me]$ cluster, **38**, are shown in Scheme 5.

The orbital interactions describing the σ(Ru−C) bonds are indicative for a μ-carbenic interaction among the carbon atoms and Ru(II) centers; thereby, the C_3 ring adopts a resonance form between μ-carbene and μ_3-cyclopropenyl. Furthermore, the large bent-back angles of the substituent on the C_3 ring are also consistent with the μ-carbenic character of the C_3 ring carbon atoms.

Mechanistic Aspects of the Cleavage of the N−H Bonds of NH_3 by the [*cyclo*-$Ru_3(\mu\text{-H})_3]^{3+}$ Cluster. To understand and advance the performance of the [*cyclo*-$Ru_3(\mu\text{-H})_3]^{3+}$ cluster in the activation of C−H, N−H, O−H, H−H, C−C, and C═C bonds, the geometric and energetic reaction profile of the activation of the N−H bonds of NH_3 has been monitored by means of B3P86/lanl2dz(Ru)∪6-31G**(H,N) calculations. The predicted geometric and energetic reaction profile are depicted schematically in Figure 8. Structural details of the equilibrium structures of the intermediates and transition states are given in Figure S2. The reaction of NH_3 (1 atm) with $[Cp^*Ru)_3(\mu\text{-H})_3\text{-}(\mu_3\text{-H})_2]$ in a sealed tube at 80 °C reached its equilibrium after standing for 3 days.[1o]

The first stage of the activation process involves coordination of NH_3 ligand to a Ru metal center of the [*cyclo*-$Ru_3(\mu\text{-H})_3]^{3+}$ cluster yielding intermediate **39**. The formation of intermediate **39** was calculated to be exoergic by −71.9 kcal/mol. In the next step, intramolecular migration of a hydrogen atom to adjacent Ru metal center occurs through $\mathbf{TS_{39-40}}$ yielding intermediate **40** involving a terminal amido group with an activation barrier 27.1 kcal/mol. In the vibrational mode corresponding to the imaginary frequency of $\mathbf{TS_{39-40}}$, the dominant motions involve the transferring hydrogen atom. Intermediate **40** is transformed easily to intermediate **41** involving a μ_2-amido bridge via $\mathbf{TS_{40-41}}$ surmounting a very low activation barrier of 5.0 kcal/mol. The transformation process is exoergic by −18.1 kcal/mol. The calculated structure of the μ_2-amido bridged intermediate **41** involved in the activation process closely resembles the experimental structure of the $[(C_5Me_5)_3Ru_3(\mu\text{-H})_3(\mu_2\text{-NH}_2)]$ intermediate reported very recently by Suzuki and co-workers.[31] The authors elucidated that hydrogenation of triruthenium μ_3-imido complex $[(C_5Me_5)_3\text{-}Ru_3(\mu\text{-H})_3(\mu_3\text{-NH})]$ proceeds through homolytic cleavage of dihydrogen. However, the reaction path for further hydrogenation of the μ_3-imido complex $[(C_5Me_5)_3Ru_3(\mu\text{-H})_3(\mu_3\text{-NH})]$ to form $[(C_5Me_5)_3Ru_3(\mu\text{-H})_3(\mu_3\text{-H})_2]$ and ammonia still remains unclear. This reaction path corresponds to the next step of the aforementioned activation process that corresponds to an intramolecular migration of a second hydrogen atom from the amido bridge to a Ru central atom affording intermediate **42**, which involves a triply bridged μ_3-imido group and a loosely η^2-coordinated dihydrogen molecule, which is easily detached to yield the final product **22**. The migration of the second hydrogen atom proceeds via $\mathbf{TS_{41-42}}$, surmounting an energy barrier of 25.4 kcal/mol, which is comparable to that of the first hydrogen migration step. The two hydrogen migration steps are predicted to be the rate-limiting steps for both the forward and the reverse reactions. In the vibrational mode corresponding to the imaginary frequency of $\mathbf{TS_{41-42}}$, the dominant motions involve the migrating hydrogen atom along with the detachment of the coordinated dihydrogen. It is worth noting that the whole N−H bond activation process of NH_3 by the [*cyclo*-$Ru_3(\mu\text{-H})_3]^{3+}$ cluster is exothermic, the exothermicity being −71.3 kcal/mol.

Conclusions

In this paper, we have demonstrated, using electronic structure calculation methods (DFT), that the versatile chemical reactivity of the antiaromatic [*cyclo*-$Ru_3(\mu_2\text{-H})_3]^{3+}$ molecule related with the activation of small molecules that leads to the breaking of various strong single and double bonds seems to be primarily owing to the predicted high antiaromatic character of the molecule. The results can be summarized as follows:

(31) Kameo, H.; Nakajima, Y.; Suzuki, H. *Eur. J. Inorg. Chem.* **2007**, 1793.

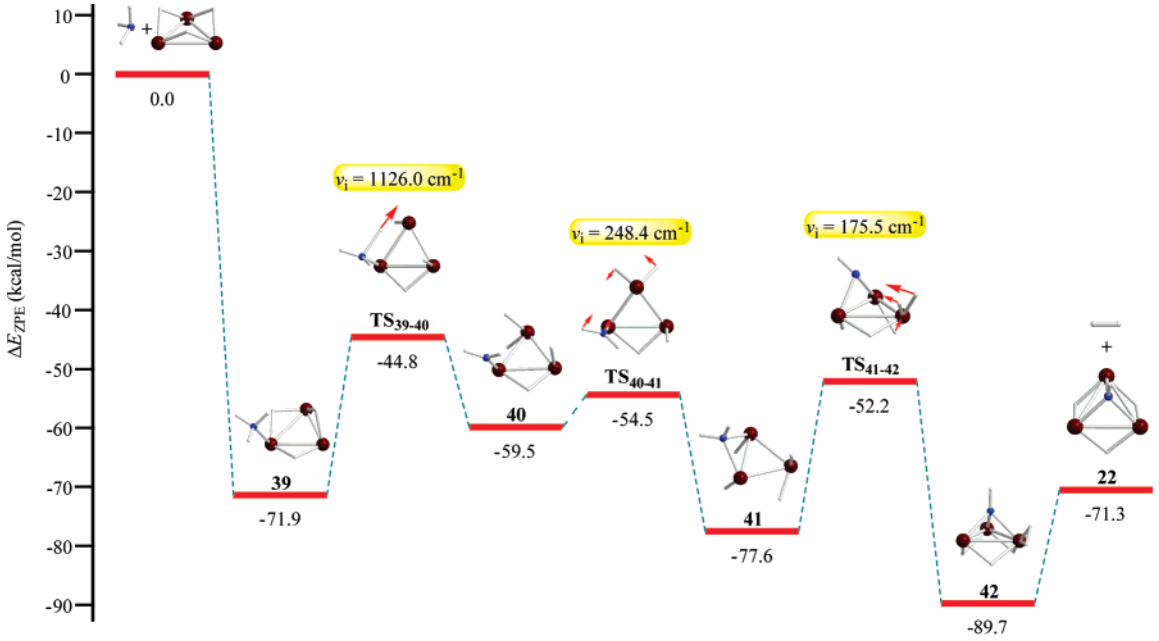

Figure 8. Geometric and energetic reaction profile of the activation of the N−H bonds of NH_3 by the [*cyclo*-$Ru_3(\mu$-$H)_3]^{3+}$ cluster yielding the [*cyclo*-$Ru_3(\mu$-$H)_3(\mu_3$-$NH)]^{3+}$ cluster computed at the B3P86/lanl2dz(Ru)∪6-31G**(H,N) level of theory.

A series of novel prototypical ligand stabilized [*cyclo*-$Ru_3(\mu_2$-$X)_3]^{0,3+}$ (X = H, BH, CH_2, NH_2, OH, Cl, NH, CO, O, PH_2, CF_2, CCl_2, CNH, N_3) isocycles have been thoroughly investigated by means of electronic structure calculation methods at the DFT level. In all [*cyclo*-$Ru_3(\mu_2$-$X)_3]^{0,3+}$ molecules, except of the cluster with X = CCl_2, the X ligands bridge symmetrically neighboring ruthenium atoms forming isosceles Ru(μ-X)Ru tiangles that are aligned on the one side of the equilateral Ru_3 triangle. This is exactly the conformation adopted by trinuclear arene ruthenium polyhydrido clusters studied experimentally so far, illustrating that the stabilizing cyclopentadiene or benzene coligands do not affect the $Ru_3(\mu_2$-$X)_3$ core structure.

All [*cyclo*-$Ru_3(\mu_2$-$X)_3]^{0,3+}$ molecules are predicted to be bound with respect to their dissociation to "free" Ru^{2+} and $[X]^{0,1-,2-}$ moieties in their ground states. Moreover, all neutral species are predicted to be bound with respect to dissociation to their RuX monomeric species, while the cationic clusters are predicted to be unbound.

The bonding in the 3-membered ruthenium rings is characterized by a common ring-shaped electron density, more commonly seen in aromatic organic molecules and in "all-metal" aromatics. The Ru_3 ring structural core exhibits a composite bonding mode involving σ-, π-, and δ-type MOs. However, there is a striking difference in the shape of the cyclic delocalization of the electron density of the aromatic Ru_3 isocycles and the aromatic cyclopropenium cation, due to the alignment of the bridging ligands X on the one side of the Ru_3 plane forming a triangle parallel to the Ru_3 triangle in a staggered conformation. This alignment perturbs the cyclic electron cloud on the two sides of the Ru_3 ring by distending the electron cloud found in the opposite side. Therefore, the cyclic delocalization on the two sides of the Ru_3 ring is not equivalent, and consequently, the induced ring current on each side of the Ru_3 ring would be different. The aromaticity/antiaromaticity of the model [*cyclo*-$Ru_3(\mu_2$-$X)_3]^{0,3+}$ isocycles was verified by the magnetic criterion of aromaticity/antiaromaticity of a molecule, that of the nucleus-independent chemical shift, NICS(0), NICS(1), NICS(−1), $NICS_{zz}(1)$, and $NICS_{zz}(-1)$, along with the NICS scan profiles. All [*cyclo*-$Ru_3(\mu_2$-$X)_3]^{0,3+}$ species, except for the [*cyclo*-$Ru_3(\mu_2$-$H)_3]^{3+}$ species, are predicted to be aromatic molecules. The NICS scan pictures clearly shows the dramatic change of the aromaticity/antiaromaticity on the two sides of the Ru_3 ring. This change could be explained on the grounds of the different coordination environment above and below the Ru_3 ring.

The versatile chemical reactivity of the antiaromatic [*cyclo*-$Ru_3(\mu_2$-$H)_3]^{3+}$ molecule is related with the activation of small molecules that leads to the breaking of various strong single and double bonds and the formation of face-capping moieties coordinated to the Ru_3 ring in μ_3-fashion. The molecular and electronic structures, stabilities, and bonding features of a series of [*cyclo*-$Ru_3(\mu_2$-$H)_3(\mu_3$-$Nuc)]^{0,1,2+}$ (Nuc = BH, BCN, BOMe, C^{4-}, CH^{3-}, CMe^{3-}, N^{3-}, NH, N_3^-, NCO^-, OCN^-, NCS^-, O^{2-}, S^{2-}, OH^-, P^{3-}, POH^{2-}, Cl^-, O_2^{2-}, NCH, AlMe, GaMe, C_6H_6, and *cyclo*-C_3H_2Me) products formed upon reacting the archetype [*cyclo*-$Ru_3(\mu_2$-$H)_3]^{3+}$ molecule with the appropriate substrates were investigated by means of electronic structure computational techniques. Generally, in the [*cyclo*-$Ru_3(\mu$-$H)_3(\mu_3$-$Nuc)]^q$ molecules, the nucleophile Nuc is coordinated to the Ru_3 ring in a μ_3-Nuc coordination mode, capping the face of the ring from the most antiaromatic side, which is the side opposite to that of the bridging hydride ligands. This is exactly the case for the "actual" $[(\eta^5$-$C_5Me_5)_3Ru_3(\mu$-$H)_3(\mu_3$-$Nuc)]^q$ and $[(\eta^6$-$C_6Me_6)_2(\eta^6$-$C_6H_6)Ru_3(\mu$-$Nuc)]^q$ molecules that have been extensively studied experimentally. All [*cyclo*-$Ru_3(\mu_2$-$H)_3(\mu_3$-$Nuc)]^{0,1,2+}$ molecules are predicted to be bound with respect to their dissociation to the parent [*cyclo*-$Ru_3(\mu$-$H)_3]^{3+}$ species and the "free" nucleophile in their ground states.

Finally, the mechanistic details for a representative activation process, the dehydrogenation of NH_3 to yield a face-capping imido-group (μ_3-NH) to the Ru_3 ring, were delineated by calculating the geometric and energetic reaction profile of the activation process.

Supporting Information Available: Complete ref 7. NICS scan pictures of the [*cyclo*-$Ru_3(\mu_2\text{-}X)_3]^{0.3+}$ molecules are shown in Figure S1. Structural details of the equilibrium structures of the intermediates and transition states of the activation of the N−H bonds of NH_3 by the [*cyclo*-$Ru_3(\mu\text{-}H)_3]^+$ cluster are given in Figure S2. The composition of the $Ru_3(\mu_3\text{-}Nuc)$ natural bonds of the [*cyclo*-$Ru_3(\mu\text{-}H)_3(\mu_3\text{-}Nuc)]^q$ clusters are compiled in Table S1. The Cartesian coordinates and energies of all stationary points are compiled in Tables S2 and S3, respectively. This information is available free of charge via the Internet at http://pubs.acs.org.

JA074094P